catalysts

MDPI

Review

Recent Modification Strategies of MoS_2 towards Electrocatalytic Hydrogen Evolution

Lei Liu, Ning Liu *, Biaohua Chen, Chengna Dai and Ning Wang

College of Environmental Science and Engineering, Beijing University of Technology, Beijing 100124, China; b202165064@emails.bjut.edu.cn (L.L.); chenbh@bjut.edu.cn (B.C.); daicn@bjut.edu.cn (C.D.); ning.wang.1@bjut.edu.cn (N.W.)

* Correspondence: liuning@bjut.edu.cn

Abstract: Hydrogen production by the electrolysis of water is a green and efficient method, which is of great significance for achieving sustainable development. Molybdenum disulfide (MoS_2) is a promising electrocatalyst for hydrogen evolution reaction (HER) due to its high electrochemical activity, low cost, and abundant reserves. In comparison to the noble metal Pt, MoS_2 has poorer hydrogen evolution performance in water electrolysis. Therefore, further modifications of MoS_2 need to be developed aiming at improving its catalytic performance. The present work summarizes the modification strategies that have been developed in the past three years on hydrogen evolution from water electrolysis by utilizing MoS_2 as the electrocatalyst and following the two aspects of internal and external modifications. The former includes the strategies of interlayer spacing, sulfur vacancy, phase transition, and element doping, while the latter includes the heterostructure and conductive substrate. If the current gap in this paper's focus on modification strategies for electrocatalytic hydrogen evolution in water electrolysis is addressed, MoS_2 will perform best in acidic or alkaline media. In addition to that, the present work also discusses the challenges and future development directions of MoS_2 catalysts.

Keywords: hydrogen evolution reaction; molybdenum disulfide; modification strategies

Citation: Liu, L.; Liu, N.; Chen, B.; Dai, C.; Wang, N. Recent Modification Strategies of MoS_2 towards Electrocatalytic Hydrogen Evolution. *Catalysts* **2024**, *14*, 126. https://doi.org/10.3390/catal14020126

Academic Editor: Maria A. Goula

Received: 4 January 2024
Revised: 29 January 2024
Accepted: 1 February 2024
Published: 5 February 2024

1. Introduction

The massive consumption of fossil fuels has caused a series of environmental problems and also led to energy depletion [1–3]. The development of green and pollution-free energy has become an important task of contemporary scientific research. Hydrogen energy is a clean, efficient, and renewable energy source with broad application prospects. At present, hydrogen is mainly produced through methane steam reforming and coal gasification, but it requires fossil energy as raw materials, and CO_2 is emitted during the production process, which causes environmental pollution [4]. Hydrogen production by the electrolysis of water is an important clean energy production method, which provides an environmentally friendly and sustainable method for hydrogen energy production. The electrolysis of water is composed of two half-reactions: hydrogen evolution reaction at the cathode, and oxygen evolution reaction at the anode [5–8]. Problems, such as high overpotential and high energy consumption caused by the cathodic polarization of electrolyzed water, limit its industrial application. In order to improve the efficiency of hydrogen production by electrolysis of water, and reduce process costs, it is necessary to develop efficient cathode catalysts to reduce the overpotential of the reaction [9]. At present, the most effective catalyst for electrolytic water hydrogen evolution is the noble metal Pt, but the high cost and low reserves limit its large-scale application [10,11]. Therefore, there is an urgent need to develop high-performance HER catalysts with a low cost and abundant reserves.

MoS_2 has become the focus of research due to its low cost, unique structure, and properties [12–14]. According to the arrangement of atomic layers, MoS_2 can generally be

divided into a thermodynamically stable 2H phase and a metastable 1T phase [15,16]. In nature, MoS_2 exists in the 2H phase, which has a two-dimensional lamellar structure similar to graphite, and the layers are connected by van der Waals forces [17]. The monolayer consists of three layers of S-Mo-S atoms, in which two layers of S atoms are symmetrically arranged, while the Mo atom is in the center of the triangular prism formed by S atoms, and is coordinated with the surrounding six S atoms [18]. The "H" in 2H-phase MoS_2 represents the coordination structure of this hexagonal crystal system, and the "2" represents the structural period, that is, two layers of S-Mo-S molecular layers are repeatedly stacked as a structural unit. The 1T-phase MoS_2 also has a two-dimensional structure. The monolayer is composed of three layers of S-Mo-S atoms, and Mo is sandwiched between two layers of S atoms [17]. However, unlike the 2H phase, in the 1T phase, two layers of S atoms are arranged asymmetrically. Its structure can be described as a result of rotating one layer of S atoms by 60° with the center of the top plane as the rotation center based on the triangular prism structure in the 2H phase [19]. Therefore, the Mo atom in 1T-phase MoS_2 is in octahedral coordination with the surrounding six S atoms, corresponding to the "T" in 1T, which means "Trigonal" [18]. Along the c-axis direction, 1T-phase MoS_2 is repeatedly stacked with a single atomic layer as a unit, corresponding to the "1" in 1T. MoS_2 has good HER activity, but due to its low conductivity and inert basal plane, its performance still lags far behind that of Pt catalysts [20]. In order to further improve the performance of MoS_2 in the electrolysis of water for hydrogen evolution, researchers have adopted a variety of regulation strategies, such as inducing phase transitions [21–23], manufacturing defects [24–26], doping elements [27–29], and constructing a heterostructure [30–32]. These strategies can optimize the key factors that limit the hydrogen evolution performance of electrolytic water, such as the density of the catalytic active site, conductivity, Gibbs free energy of hydrogen adsorption (ΔG_H), etc. The ΔG_H is an important parameter to evaluate the HER catalyst, and the ΔG_H corresponding to an ideal HER catalyst should be close to zero [28,33].

This work summarizes the modification strategies of MoS_2 in the past three years and divides the modification strategies into internal modification and external modification according to whether the original structure has changed. Internal modification refers to methods such as increasing the interlayer spacing, introducing sulfur vacancies, inducing phase transition, and doping elements, while external modification refers to methods such as constructing heterostructures and introducing conductive substrates. Examples are provided for each method. If the modification strategies involved in this work can be fully utilized, the HER performance of MoS_2 in acidic or alkaline electrolytes will be the best. Finally, this work discusses the challenges and development directions in developing high-performance MoS_2 catalysts.

2. Internal Modification

2.1. Interlayer Spacing

Abundant active sites can play a crucial role in the HER. The expanded interlayer spacing of MoS_2 is beneficial to exposing more active sites and causes the rapid transfer of protons/electrons and the ready release of hydrogen [34]. In addition, the expanded interlayer spacing can optimize the ΔG_H at the edge and basal plane of MoS_2, promoting the adsorption of surface H and the desorption of hydrogen, which thereby can effectively improve the HER performance of the material [35].

Zhang et al. [36] stirred the solution mixture containing DMF at room temperature and obtained Mo-MOF at 120 °C, which was heated to 200 °C and converted into 200-1T-MoS_2. Under the stress of N, N-dimethylformamide oxide, the interlayer spacing of 200-1T-MoS_2 was extended to 10.87 Å (Figure 1a). It has an overpotential of 98 mV at 10 mA cm^{-2} and a Tafel slope of 52 mV dec^{-1} (Figure 1b,c). Theoretical calculations show that the enlarged crystal plane changes the electronic structure of 1T-MoS_2 and reduces the adsorption–desorption potential of protons (Figure 1d) so that 200-1T-MoS_2 exhibits efficient HER activity.

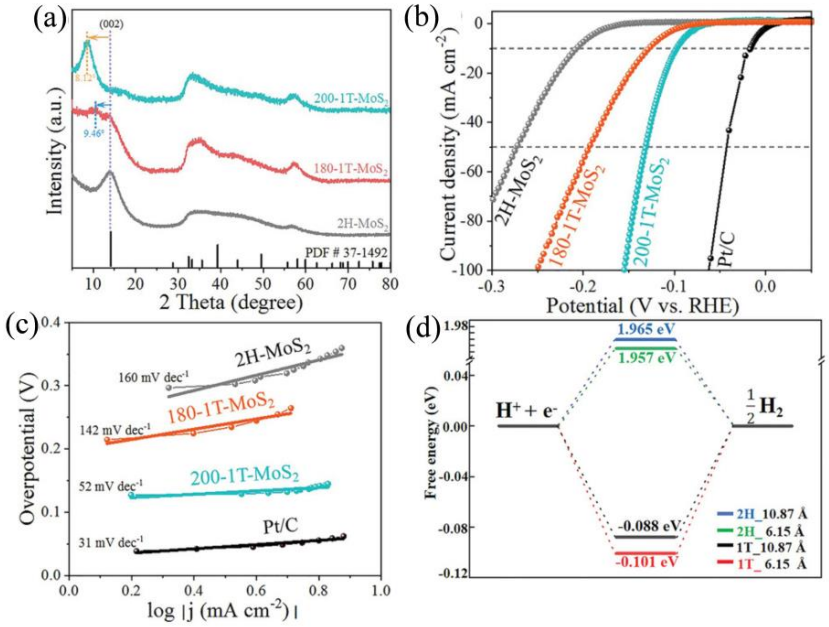

Figure 1. (**a**) XRD diffraction patterns of 2H-MoS_2, 180-1T-MoS_2, and 200-1T-MoS_2. (**b**) Polarization curves and (**c**) corresponding Tafel slopes of 2H-MoS_2, 180-1T-MoS_2, and 200-1T-MoS_2 in 0.5 M H_2SO_4. (**d**) ΔG_H of 2H-MoS_2 and 1T-MoS_2 with interlayer spacings of 6.15 and 10.87 Å, respectively. Reproduced with permission from Ref. [36], Copyright 2023, Wiley.

Hu et al. [37] used $Na_2MoO_4{\cdot}2H_2O$ and C_2H_5NS as raw materials to synthesize 1T/2H-MoS_2/NH_4^+-200 with an interlayer spacing of 0.94 nm under reaction conditions of 200 °C (Figure 2a). They attributed the increase in interlayer spacing to the entry of ammonium ions during the reaction. The increased interlayer spacing is beneficial to the full exposure of the active site and also provides a large channel for ion transport. The 1T/2H-MoS_2/NH_4^+-200 exhibited excellent HER performance with an overpotential of 159.9 mV at 10 mA cm^{-2} and a Tafel slope of 55.5 mV dec^{-1} in 0.5 M H_2SO_4 (Figure 2b,c). In addition, 1T/2H-MoS_2/NH_4^+-200 also had excellent electrochemical stability. After 1000 cyclic voltammetry (CV) cycles, the overpotential of 10 mA cm^{-2} only dropped by 7.2 mV.

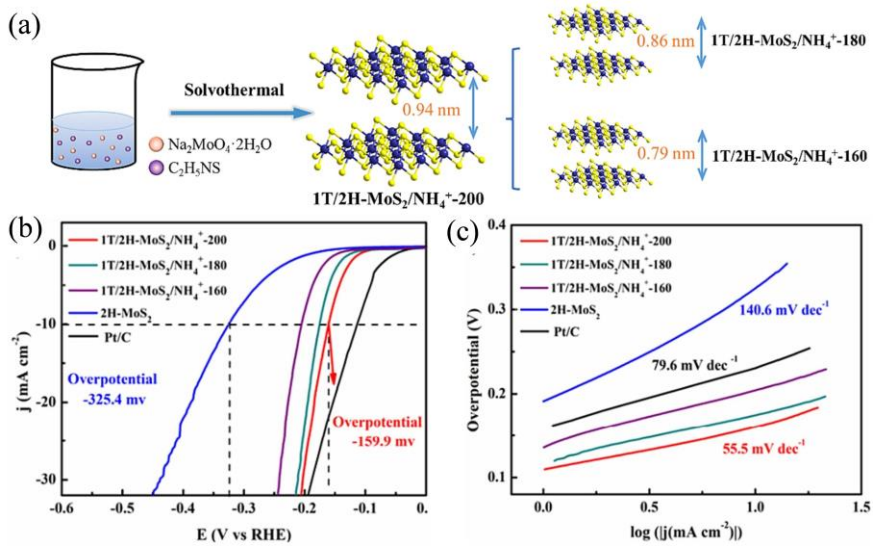

Figure 2. (**a**) Schematic illustration of the synthetic method for catalysts. (**b**) Polarization curves and (**c**) corresponding Tafel slopes of catalysts in 0.5 M H_2SO_4. Reproduced with permission from Ref. [37], Copyright 2023, Elsevier.

In addition to the methods mentioned in the above examples, other methods of increasing the interlayer spacing of MoS_2 have also been reported in the literature [35,38,39]. Jin et al. [35] used H_2 as a structural directing agent to synthesize Co-MoS_2-1.4 with an interlayer spacing of 10.3 Å, which presents a low overpotential of 56 mV at 10 mA cm^{-2} and a Tafel slope of 32 mV dec^{-1}. Gao et al. [38] used a microwave-assisted strategy to obtain MoS_2 with an interlayer spacing of 9.4 Å, which has excellent HER performance with an overpotential of 149 mV at 10 mA cm^{-2} and a Tafel slope of 49 mV dec^{-1}. Bui et al. [39] generated graphene in situ and inserted it into the MoS_2 layers to obtain MoS_2@Gr with an expanded interlayer spacing (9.6 Å) and a significantly improved HER performance compared with MoS_2.

Extending the interlayer spacing to improve the HER performance of MoS_2 has attracted widespread attention. However, the types of foreign species that support the interlayer expansion of MoS_2 and the process of foreign species entering the interlayer gap are not clear. Answering these questions definitively is crucial to developing methods to precisely regulate the interlayer spacing of MoS_2. Therefore, future research needs to utilize in situ techniques to track the formation process of interlayer expanded MoS_2 in real-time. Real-time measurements can provide new kinetic information and help us understand the origin of MoS_2 interlayer expansion.

2.2. Sulfur Vacancy

In the research on hydrogen evolution in electrolytic water from MoS_2, sulfur vacancies are one of the important research directions [40,41]. Sulfur vacancies refer to vacancies formed by the absence of some sulfur atoms in the MoS_2 crystal lattice. The defect structure is considered to have good catalytic activity in the field of electrocatalysis, especially in water-splitting reactions. Generating sulfur vacancy defects is an effective MoS_2 modification strategy, which can activate the inert basal plane by generating a new interstitial state close to the Fermi level, so as to optimize the active site and improve the HER performance of MoS_2 [42].

The formation of sulfur vacancies is generally achieved through post-treatment processes. Gu et al. [42] used H_2O_2 to etch 2H-MoS_2 and obtained SV-2H-MoS_2 nanosheets containing abundant sulfur vacancies. HAADF-STEM intuitively shows that there are abundant sulfur vacancies on the surface of SV-2H-MoS_2 (Figure 3a). The EPR signal intensity of SV-2H-MoS_2 is significantly higher than that of 2H-MoS_2, indicating that the sulfur vacancy density on the surface of SV-2H-MoS_2 is much higher than that of 2H-MoS_2 (Figure 3b). Figure 3c,d shows that the overpotential of SV-2H-MoS_2 containing abundant sulfur vacancies is 369 mV (@10 mA cm^{-2}), and the Tafel slope is 68.7 mV dec^{-1}, which is significantly lower than that of 2H-MoS_2 (686 mV@10 mA cm^{-2} and 204.1 mV dec^{-1}). It indicates that the generation of sulfur vacancy can significantly improve the HER performance of SV-2H-MoS_2.

The salt-assisted chemical vapor deposition (CVD) can be used to directly prepare MoS_2 containing abundant sulfur vacancies. Man et al. [43] synthesized a monolayer of MoS_2 by the CVD method using $Na_2MoO_4 \cdot 2H_2O$ and sulfur vapor as Mo and S sources, and SiO_2/Si as a substrate. By treating the substrate through the spraying of KCl solutions of different concentrations, the number of sulfur vacancies in the MoS_2 basal plane can be adjusted. As shown in Figure 4a, the higher the concentration of KCl solution sprayed on the substrate, the more sulfur vacancies in MoS_2, and the MoS_2-2.5 obtained after treating the substrate with 2.5 M KCl solution contains the most abundant sulfur vacancies (3.35×10^{14} cm^{-2}). Figure 4b,c shows that the overpotential of MoS_2-2.5 is 90 mV at 10 mA cm^{-2} and the Tafel slope is 54.3 mV dec^{-1} in 0.5 M H_2SO_4, which is significantly lower than that of the original MoS_2-0 (220 mV@10 mA cm^{-2} and 211.95 mV dec^{-1}). Compared with MoS_2-0, the significantly improved HER performance of MoS_2-2.5 can be attributed to the abundant sulfur vacancies on the basal plane. Figure 4d shows that the ΔG_H of the V_{2S} and the V_S are −0.13 eV and −0.06 eV, respectively, which significantly improves the HER

activity of the inert basal plane, indicating that the abundant sulfur vacancies in MoS_2 have good catalytic efficiency.

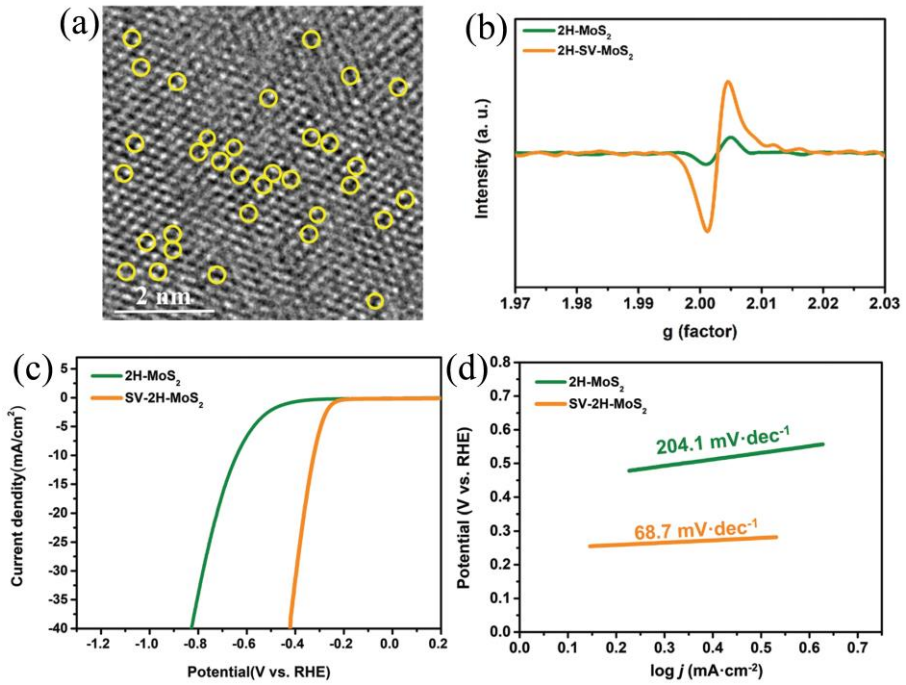

Figure 3. (**a**) HRTEM image of SV-2H-MoS_2. (**b**) Electron paramagnetic resonance (EPR) patterns of 2H-MoS_2 and SV-2H-MoS_2. (**c**) Polarization curves and (**d**) corresponding Tafel slopes of 2H-MoS_2 and SV-2H-MoS_2 in 0.5 M H_2SO_4. Reproduced with permission from Ref. [42], Copyright 2023, Wiley.

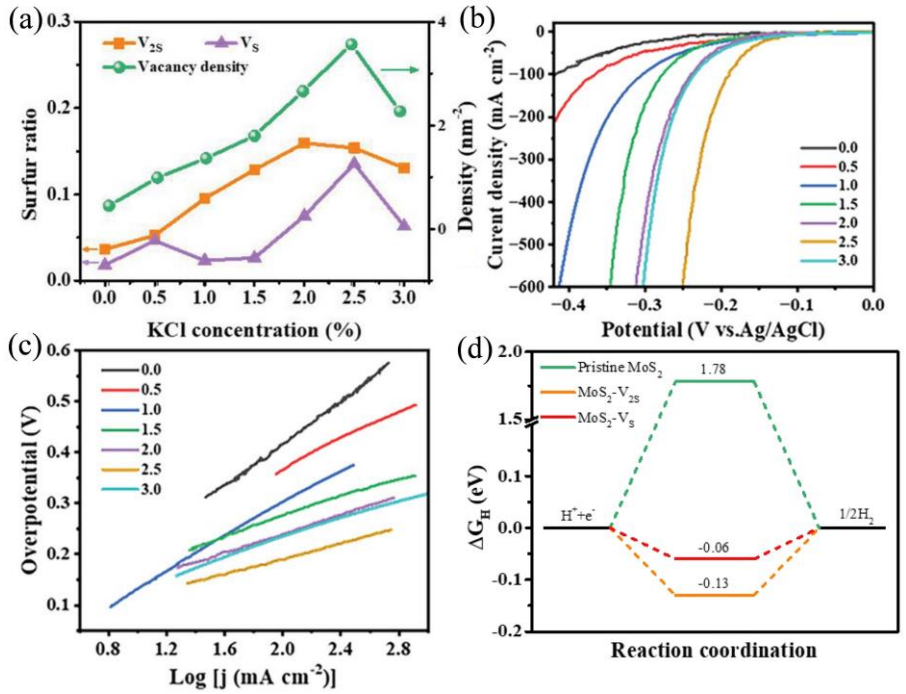

Figure 4. (**a**) Statistics of surface sulfur vacancy density (green line), single sulfur vacancy (V_S, purple line), and double sulfur vacancy (V_{2S}, orange line) of MoS_2 under different KCl concentrations. (**b**) Polarization curves and (**c**) corresponding Tafel slopes of catalysts in 0.5 M H_2SO_4. (**d**) Adsorption free energies of H atoms of pristine MoS_2, MoS_2-V_{2S}, and MoS_2-V_S. Reproduced with permission from Ref. [43], Copyright 2023, Wiley.

In addition to the above H_2O_2 etching and CVD methods, other methods are often used to generate sulfur vacancies in the MoS_2 [26,44,45]. Ye et al. [44] obtained MoS_2 with rich sulfur vacancies by H_2 annealing, and these sulfur vacancy defects significantly improved the HER performance of MoS_2. Tsai et al. [26] used the electrochemical desulfurization method to remove sulfur atoms on the surface of MoS_2. They controlled the extent of desulfurization by regulating the desulfurization potential, thereby improving the HER activity of MoS_2. Li et al. [45] used Ar plasma to treat MoS_2 samples and obtained SV-MoS_2 containing abundant sulfur vacancies, which has good HER performance with an overpotential of 170 mV at 10 mA cm^{-2} and a Tafel slope of 60 mV dec^{-1}.

Man et al. [43] have demonstrated that single sulfur vacancies and double sulfur vacancies in MoS_2 have different effects on HER. The effect of other types of sulfur vacancies on HER is not clear. At present, most of the methods for generating sulfur vacancies are to generate sulfur vacancies at the basal plane and edge of MoS_2 at the same time. It is impossible to accurately control the position of sulfur vacancy generation, and there is a lack of research on the effect of sulfur vacancies on the basal plane or edge of MoS_2 on HER. Therefore, future research on sulfur vacancies should focus on these issues.

2.3. Phase Transition

Figure 5 shows the 2H and 1T phases of MoS_2, and the different crystalline phases of MoS_2 exhibit diverse properties. The 2H-phase MoS_2 has semiconductor properties and has a band gap with a length of 1.2~1.9 eV near the Fermi level; the 1T-phase MoS_2 has the properties of metal conductor, no band gap near the Fermi level, and thereby has good conductivity [46,47]. The basal plane of the 2H-phase MoS_2 is inert, and only the Mo edges are active for the HER [48–52]. Different from 2H-phase MoS_2, the active sites of 1T-phase MoS_2 are mainly located on the basal plane, and the Mo edge contributes relatively little to the overall HER efficiency. The basal plane of 1T-phase MoS_2 has a much larger active surface area than the edge, thus ensuring a higher HER activity [53,54]. Creating a high proportion of 1T-phase MoS_2 is of great significance for improving catalytic activity.

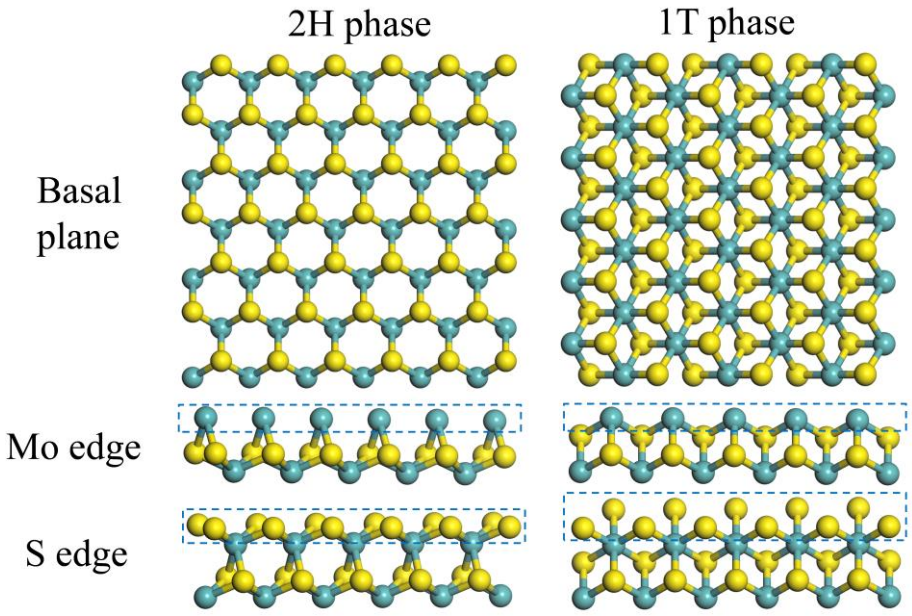

Figure 5. Ball and stick models of 2H-phase and 1T-phase MoS_2 (yellow represents sulfur atoms, blue represents Mo atoms).

Wang et al. [55] developed a simple solvothermal method to synthesize 1T-phase MoS_2. They found that the reaction solvent plays a crucial role in regulating the phase state of MoS_2: the 2H MoS_2 NSH can be obtained by using water as the solvent, while the 1T MoS_2 NSP can be obtained by using ethanol as the solvent, where the corresponding

content of the 1T phase is 77.68%. (Figure 6a,b). The synthesized 1T MoS_2 NSP exhibited excellent electrocatalytic hydrogen evolution performance with an overpotential of 188 mV at 10 mA cm^{-2} and a Tafel slope of 58.47 mV dec^{-1} (Figure 6c,d).

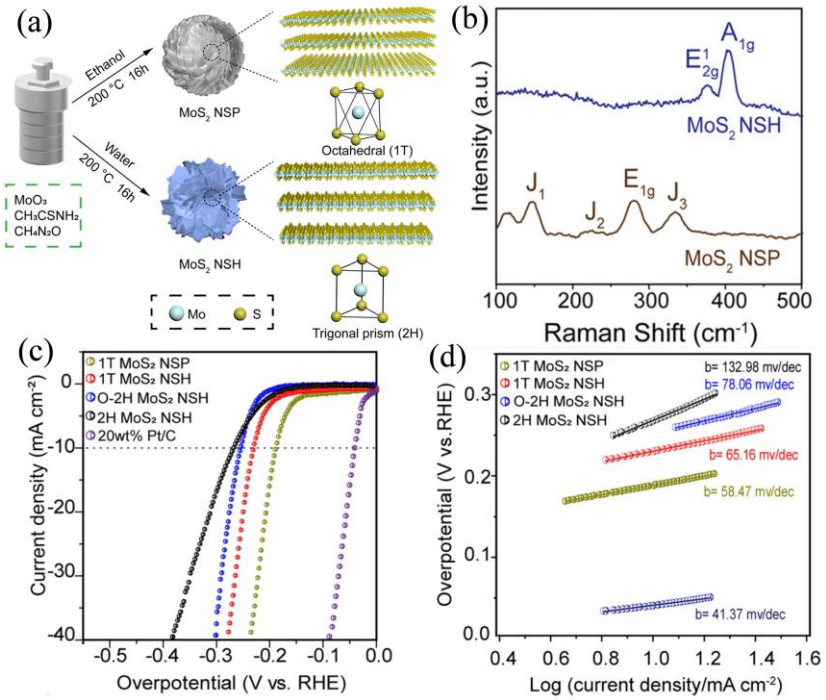

Figure 6. (**a**) Schematic illustrations of the synthesis protocols for the 1T MoS_2 NSP and 2H MoS_2 NSH. (**b**) Raman spectra of the 1T MoS_2 NSP and 2H MoS_2 NSH. (**c**) Polarization curves and (**d**) corresponding Tafel slopes of 1T MoS_2 NSP, 1T MoS_2 NSH, O-2H MoS_2 NSH, and 2H MoS_2 NSH in 0.5 M H_2SO_4. Reproduced with permission from Ref. [55], Copyright 2022, American Chemical Society.

The CVD method can also be used to synthesize MoS_2 containing a high proportion of 1T phase. Hong et al. [56] used SiO_2/Si as the growth matrix, S powder and MoO_3 as raw materials, and used the Sb_2O_3 and NaCl-assisted CVD method to synthesize MoS_2 with a 1T phase content of 61.5% (Figure 7a,b). The overpotential of the synthesized 1T-2H MoS_2 at 10 mA cm^{-2} is 212 mV, the Tafel slope is 78 mV dec^{-1}, and the electrochemical performance was significantly higher than that of 2H MoS_2 (Figure 7c,d). The S atoms at the 1T–2H phase interface are more conducive to the adsorption of H, which can improve the HER activity on the MoS_2 basal plane.

The current synthesis method obtains MoS_2 with the coexistence of a 1T phase and a 2H phase; MoS_2 containing only a 1T phase is difficult to obtain. The problem that the metastable 1T phase is easily converted to the thermodynamically stable 2H phase has not been completely solved. It is of great value to develop synthetic routes containing only 1T-phase MoS_2 and methods to maintain the stability of the 1T phase.

2.4. Element Doping

2.4.1. Metal Doping

Metal doping is an effective method to activate the inert basal of MoS_2 and enhance its catalytic activity [57,58]. Doping with metal elements can significantly change the electron density of Mo and S atoms around the doping element, thereby improving the HER activity of MoS_2 [27,28]. Commonly used doping elements include Pt, Pd, Ru, Fe, Co, Ni, and Zn [6,27,28,58,59].

Sundara Venkatesh et al. [60] synthesized Ni-MoS_2 using Na_2MoO_4, NH_2CSNH_2, and $Ni(NO_3)_2{\cdot}6H_2O$ as precursors (Figure 8a). The SEM image shows that there is no obvious agglomeration of Ni-MoS_2 nanosheets (Figure 8b). Figure 8c,d shows that the overpotential

of Ni-MoS_2 at 10 mA cm^{-2} is 302.4 mV and the Tafel slope is 66.27 mV dec^{-1}, which is significantly lower than that of MoS_2 (406.6 mV@10 mA cm^{-2} and 95 mV dec^{-1}). The EIS analysis shows that the charge transfer resistance of MoS_2 was six times higher than that of Ni-MoS_2, which indicated that Ni-doped MoS_2 achieved better charge transfer and was beneficial to improving the HER performance of MoS_2 (Figure 8e).

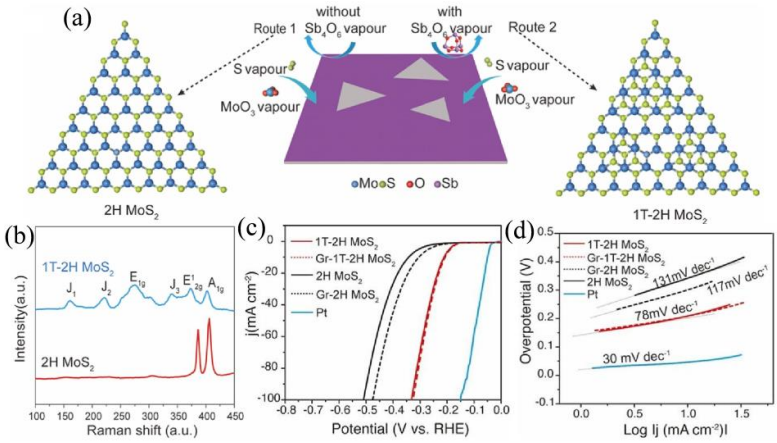

Figure 7. (**a**) Schematic illustration and atomic structure of 2H MoS_2 and 1T-2H MoS_2 grown on SiO_2/Si. Route 1 represents the growth of 2H MoS_2 nanosheets without Sb_2O_3 participation and Route 2 represents the growth of 1T-2H MoS_2 with Sb_2O_3 participation. (**b**) Raman spectra of 1T-2H MoS_2 and 2H MoS_2. (**c**) Polarization curves and (**d**) corresponding Tafel slopes of catalysts in 0.5 M H_2SO_4. Reproduced with permission from Ref. [56], Copyright 2023, Elsevier.

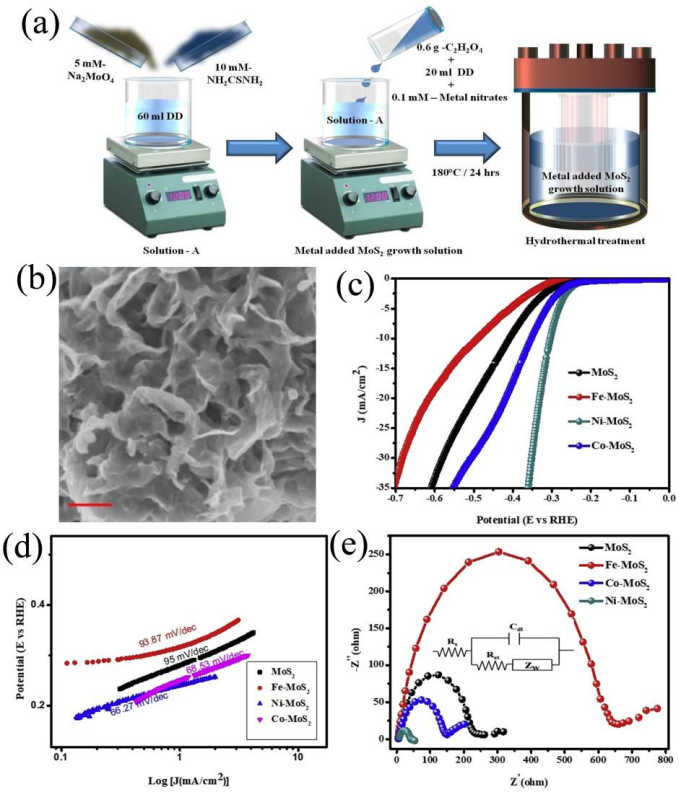

Figure 8. (**a**) Schematic illustrations of the synthesis protocols for transition metals decorated MoS_2 nanosheets. (**b**) Scanning electron microscopy (SEM) image of Ni-MoS_2 nanosheets with a uniform scale bar of 200 nm. (**c**) Polarization curves, (**d**) corresponding Tafel slopes, and (**e**) Electrochemical impedance spectroscopy (EIS) comparisons of MoS_2, Fe-MoS_2, Co-MoS_2, and Ni-MoS_2 in 0.5 M H_2SO_4. Reproduced with permission from Ref. [60], Copyright 2022, Elsevier.

Xu et al. [61] synthesized one type of Zn-1T/2H-MoS_2 with 1T and 2H phases coexisting by using $(NH_4)_6Mo_7O_{24}{\cdot}4H_2O$, CH_4N_2S, and $Zn(NO_3)_2{\cdot}6H_2O$ as precursors (Figure 9a). The 1T phase content of 1T/2H-MoS_2 was 28.2%, while the 1T phase content of Zn-1T/2H-MoS_2 increased to 46.0% after the addition of Zn (Figure 9b). The result indicated that Zn doping can lead to an increase in the 1T phase content of MoS_2, which is beneficial for improving HER performance. Figure 9c,d shows that the overpotential of Zn-1T/2H-MoS_2 is 190 mV (@10 mA cm^{-2}) and the Tafel slope is 58 mV dec^{-1}, and that the HER performance is significantly higher than that of 1T/2H-MoS_2 (237 mV@10 mA cm^{-2} and 71 mV dec^{-1}). After Zn doping, the C_{dl} of 1T/2H-MoS_2 increased from 14.2 mF cm^{-2} to 33.5 mF cm^{-2}, and the electrochemically active surface area increased from 237 cm^2 to 558 cm^2, indicating that Zn doping is beneficial to exposing more electrochemically active sites (Figure 9e).

Single-atom catalysts (SACs) have attracted widespread attention due to their maximum atomic efficiency and tunable electronic properties. Wang et al. [62] first synthesized 2H-MoS_2 through a hydrothermal method and then used 2H-MoS_2 as a substrate to load the noble metal Ru to prepare Ru@2H-MoS_2. Figure 10a,b shows that the Ru atoms exist in the form of single atoms in 2H-MoS_2. Figure 10c shows that the overpotentials of $Ru_{0.10}$@2H-MoS_2 at 10 mA cm^{-2} are 168 mV in 0.5 M H_2SO_4, respectively, which are significantly lower than those of 2H-MoS_2 (328 mV@10 mA cm^{-2}). Theoretical calculation proves that the addition of Ru significantly reduces the ΔG_H of 2H-MoS_2, which makes Ru@2H-MoS_2 exhibit excellent HER performance (Figure 10d).

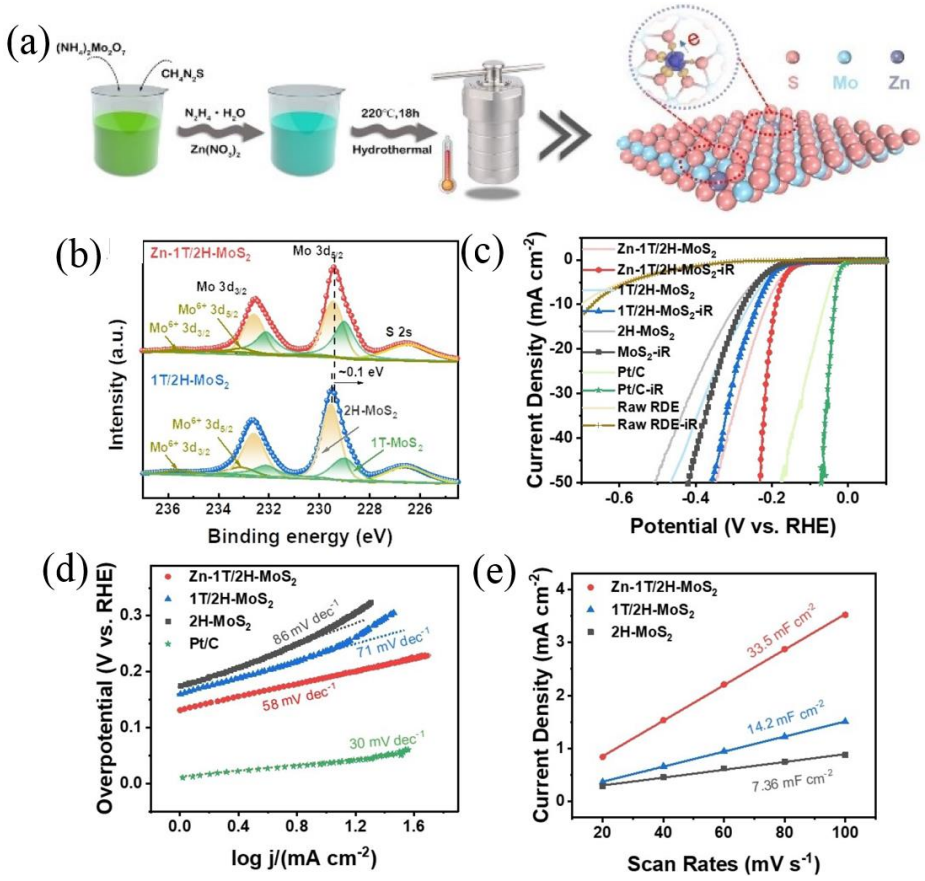

Figure 9. (**a**) Schematic illustrations of the synthesis protocols for Zn-1T/2H-MoS_2. (**b**) X-ray photoelectron spectroscopy (XPS) spectra for Mo 3d of Zn-1T/2H-MoS_2 and 1T/2H-MoS_2. (**c**) Polarization curves (lines with symbols represent the data after 100% iR-correction, the solid lines represent the data without iR-correction), (**d**) corresponding Tafel slopes (100% iR-corrected), and (**e**) the double layer capacitance (C_{dl}) of catalysts in 0.5 M H_2SO_4. Reproduced with permission from Ref. [61], Copyright 2021, Wiley.

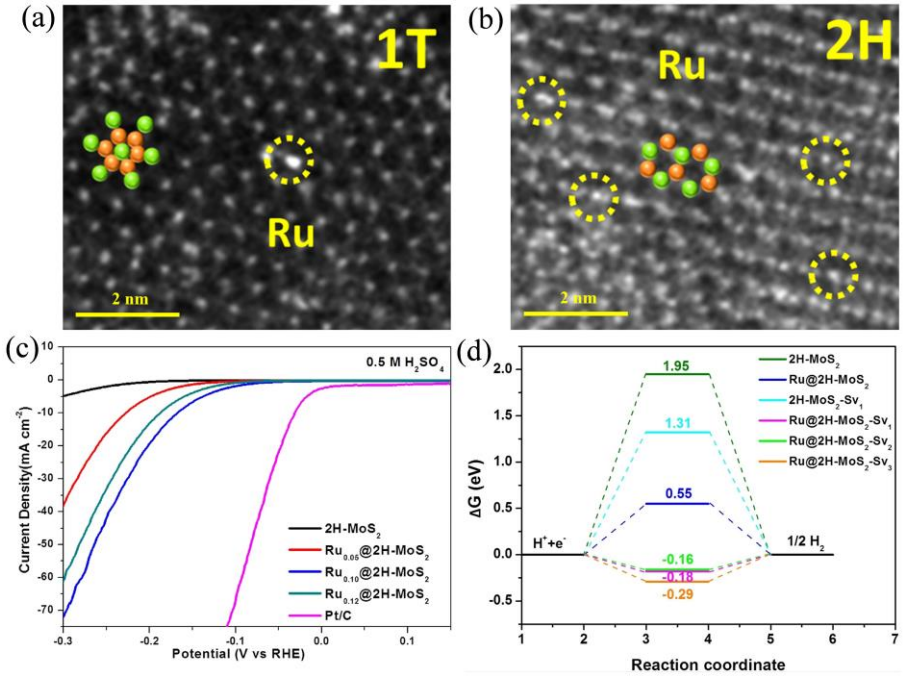

Figure 10. HRTEM images of (**a**) 1T phase and (**b**) 2H phase of $Ru_{0.10}$@2H-MoS_2. (**c**) Polarization curves of catalysts in 0.5 M H_2SO_4. (**d**) Free energy diagram for hydrogen evolution of catalysts. Reproduced with permission from Ref. [62], Copyright 2021, Elsevier.

Wang et al. [6] doped transition metals (Fe, Co, and Ni) into 1T-MoS_2 through a one-step method to improve the HER performance of 1T-MoS_2 in 1 M KOH. The overpotentials of Fe-1T-MoS_2, Co-1T-MoS_2, and Ni-1T-MoS_2 at 10 mA cm^{-2} are 269 mV, 261 mV, and 199 mV, and the Tafel slopes are 168 mV dec^{-1}, 88.5 dec^{-1}, and 52.7 dec^{-1}, and their HER performance is significantly higher than that of 1T-MoS_2 (400 mV@10 mA cm^{-2} and 237 mV dec^{-1}). Theoretical calculation shows that the doping of Fe, Co, and Ni changes the electronic structure of MoS_2, reduces the adsorption of the material to H_2O, and increases the possibility of H_2O dissociation, which is an important reason for the improvement of the HER performance of the material after metal doping MoS_2. Pei et al. [63] synthesized Pt-MoS_2 using commercial MoS_2 and H_2PtCl_6 as precursors with an overpotential of 59 mV at 10 mA cm^{-2} and a Tafel slope of 23.58 mV dec^{-1} in 0.5 M H_2SO_4. The synergistic effect between Pt nanoparticles and the edge active sites of MoS_2 increases the interlayer conductivity of MoS_2, activates the edge active sites, and significantly improves the HER performance of the material. Song et al. [64] doped Pd into 1T-MoS_2 nanorods to synthesize Pd-1T-MoS_2, which has an overpotential of 170 mV at 10 mA cm^{-2} and a Tafel slope of 98 mV dec^{-1} in 0.5 M H_2SO_4. The addition of Pd introduces more sulfur vacancies in MoS_2 and retains the 1T phase content, which is conducive to improving the HER performance of MoS_2.

2.4.2. Nonmetal Doping

The introduction of non-metallic elements, such as P, F, and N, to enhance the HER performance of MoS_2 has been proven to be effective [34,65,66]. Non-metallic dopants with different electronegativities can change the electronic structure of MoS_2 and optimize the adsorption/desorption behavior of hydrogen atoms at the active site, thereby improving the HER performance of MoS_2 [66].

The F atom has the largest electronegativity in the periodic table of elements and can cause a significant change in the electronic structure of MoS_2. Zhang et al. [66] used CHF_3 plasma to etch the edges of commercial MoS_2 on SiO_2/Si wafers and obtained etched MoS_2 with significantly increased edge sites (Figure 11a–c). Compared with the original MoS_2, the current density of etched MoS_2 increased four times at 400 mV. The overpotential of

10 mA cm^{-2} was reduced from the original 298 mV to 267 mV and the Tafel slope was reduced from the original 92 mV dec^{-1} to 65 mV dec^{-1} (Figure 11d,e), which indicated that the modification of F atoms at the edge of MoS_2 is an effective strategy to improve the HER performance of MoS_2. They also studied the ΔG_H at the edge site of MoS_2 through theoretical calculations. The ΔG_{H^*} of the etched edge is −0.26 eV, which is much smaller than the ΔG_{H^*} (−0.55 eV) of the original edge. It indicates that the addition of F weakened the excessive binding of H at the Mo sites, which is beneficial for etched MoS_2 to obtain better HER performance.

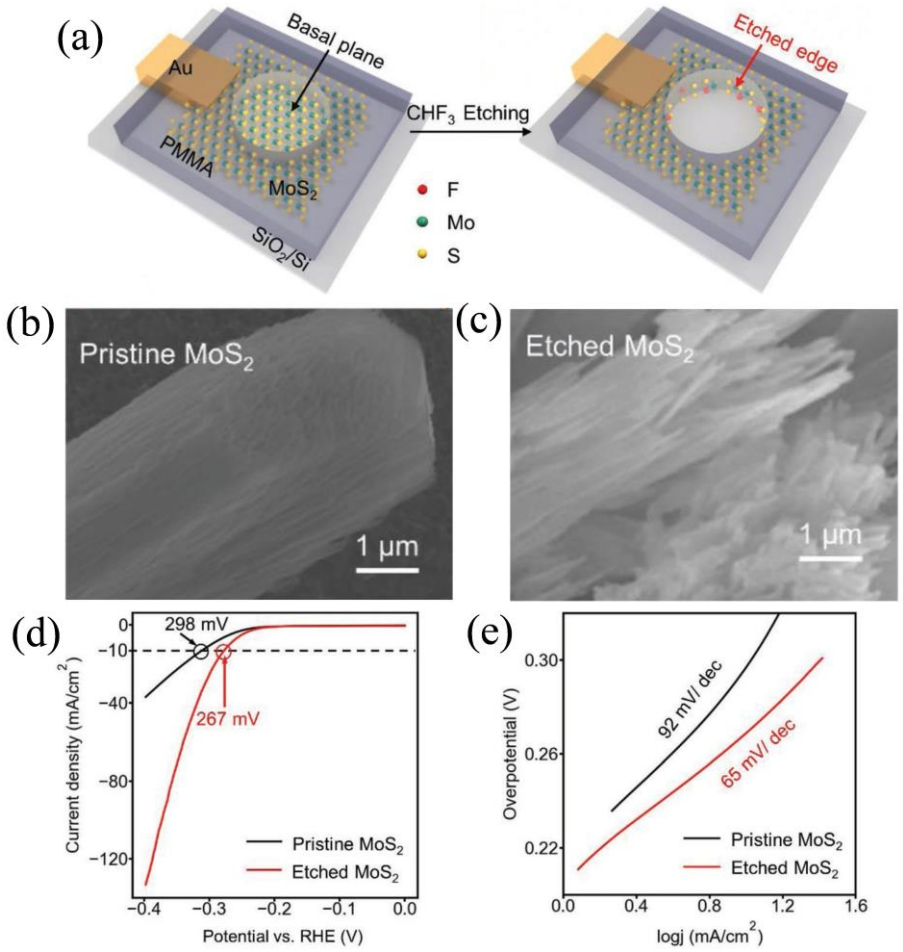

Figure 11. (**a**) Schematic illustration of in situ creating on MoS_2 by CHF_3 plasma. SEM images of (**b**) pristine MoS_2 and (**c**) etched MoS_2. (**d**) Polarization curves and (**e**) corresponding Tafel slopes of pristine MoS_2 and etched MoS_2 in 0.5 M H_2SO_4. Reproduced with permission from Ref. [66], Copyright 2021, Wiley.

The P dopant in MoS_2 can accelerate the slow HER kinetics [34]. Tian et al. [67] first synthesized MoS_2/CC using $Na_2MoO_4{\cdot}2H_2O$ and $CS(NH_2)_2$ as raw materials and the carbon cloth as the carrier. Then, using $NaH_2PO_2{\cdot}H_2O$ as the P source, P-doped P-MoS_2/CC-300 was obtained at 300 °C in a 10% H_2/Ar atmosphere (Figure 12a). XPS spectra show that the P atom doping rate of P-MoS_2/CC-300 is 2.8 wt.% (Figure 12b). Figure 12c,d shows that the overpotential and the Tafel slope of P-MoS_2/CC-300 are 81 mV (@10 mA cm^{-2}) and 98 mV dec^{-1} in 0.5 M H_2SO_4, respectively, which are significantly lower than that of MoS_2/CC-300 (135 mV@10 mA cm^{-2} and 142 mV dec^{-1}). These results suggest that the doping of P atoms can regulate the electronic interactions and optimize the electronic structure of MoS_2 to enhance the HER activity of MoS_2. In addition, P-MoS_2/CC-300 also has excellent electrochemical stability. After 3000 CV cycles, the polarization curve of the

material did not change significantly. After 15 h of stability testing, the overpotential of 10 mA cm^{-2} slightly dropped from 87 mV to 93 mV (Figure 12e).

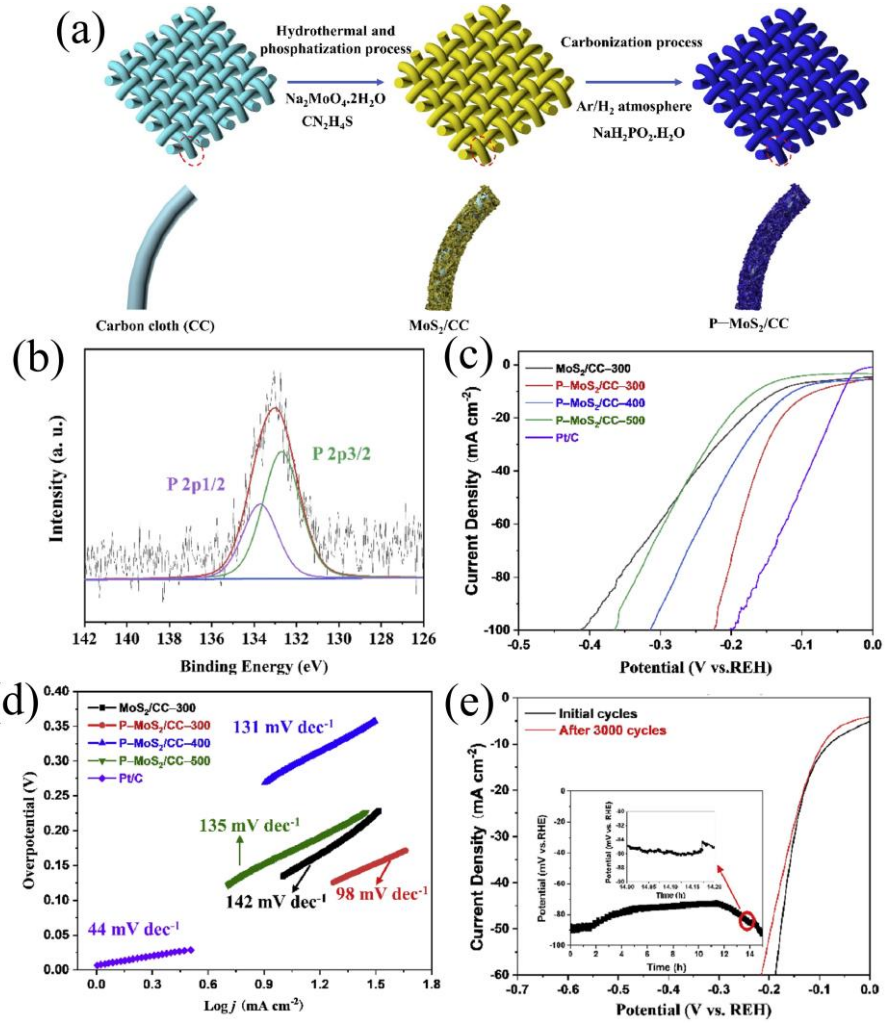

Figure 12. (**a**) Schematic illustrations of the synthesis protocols for P-MoS_2/CC. (**b**) XPS spectra of P 2p of P-MoS_2/CC-300. (**c**) Polarization curves and (**d**) corresponding Tafel slopes of MoS_2/CC-300, P-MoS_2/CC-300, P-MoS_2/CC-400, and P-MoS_2/CC-500, and (**e**) durability test of P-MoS_2/CC-300 in 0.5 M H_2SO_4. Reproduced with permission from Ref. [67], Copyright 2022, Elsevier.

Element doping can improve the HER performance of MoS_2. However, the non-noble metal elements Fe, Co, Ni, and Zn, as well as the non-metal elements F and P, can only improve the performance of MoS_2 to a limited extent, which is far behind the noble metal Pt. Although the noble metals Pt, Pd, and Ru can greatly improve the HER performance of MoS_2, they are expensive, and the actual application cost is high. The use of non-noble metal elements, or non-metal elements and noble metal elements together, can greatly improve the performance of MoS_2 while reducing the cost of the catalyst, which will be a promising road.

3. External Modification

3.1. Heterostructure

A large number of studies have proven that MoS_2-based electrocatalysts are promising non-noble metal hydrogen evolution catalysts under acidic conditions [68–70]. The high kinetic energy barrier of the initial water dissociation process, and the strong adsorption of the formed OH^- on the MoS_2 surface, lead to slow HER kinetics in alkaline solution [11]. Some researchers have focused on constructing heterostructures to accelerate the slow crack-

ing process of water by MoS_2-based catalysts in alkaline solutions [71]. Heterostructures can construct electrochemically active interfaces and enhance interfacial charge transfer dynamics by adjusting the electronic structure of the interface [72]. Due to the synergistic effect at the interface, heterostructures have excellent electrochemical properties compared to those of the single component [73,74]. Based on the advantage of each component, it is critical to rationally design the heterostructure to maximize HER performance.

Electron transfer at the heterostructure interface can optimize ΔG_H. Xiang et al. [75] synthesized 1T-MoS_2/Ni_3S_4/CC using a two-step method (Figure 13a). First, $Ni(OH)_2$ nanosheets were grown on carbon cloth to obtain $Ni(OH)_2$/CC. Then, MoS_2 nanosheets were grown on $Ni(OH)_2$ nanosheets, wherein the $Ni(OH)_2$ was gradually converted into Ni_3S_4, and, finally, 1T-MoS_2/Ni_3S_4/CC was obtained. Compared with 1T-MoS_2/CC, the Mo $3d_{5/2}$ peak of 1T-MoS_2/Ni_3S_4/CC was shifted by −0.2 eV (Figure 13b), indicating that the electron density of Mo atoms increased. Compared with Ni_3S_4/CC, the $2p_{3/2}$ peaks of Ni^{2+} and Ni^{3+} of 1T-MoS_2/Ni_3S_4/CC were shifted by +0.6 eV and +0.3 eV (Figure 13c), indicating a decrease in the number of electrons in the Ni atoms. Figure 13d shows that the overpotential of 1T-MoS_2/Ni_3S_4/CC at 10 mA cm^{-2} is 44 mV, which is significantly lower than that of 1T-MoS_2/CC (193 mV@10 mA cm^{-2}), Ni_3S_4/CC (90 mV@10 mA cm^{-2}), and $Ni(OH)_2$/CC (400 mV@10 mA cm^{-2}). The increase in the electron density of Mo atoms, and the decrease in the electron density of Ni atoms, balance the energy barriers for water dissociation and hydroxyl desorption at Ni sites, which can also optimize ΔG_H at Mo edge sites (Figure 13e–g), and the synergistic effect improves the activity of the material's alkaline HER.

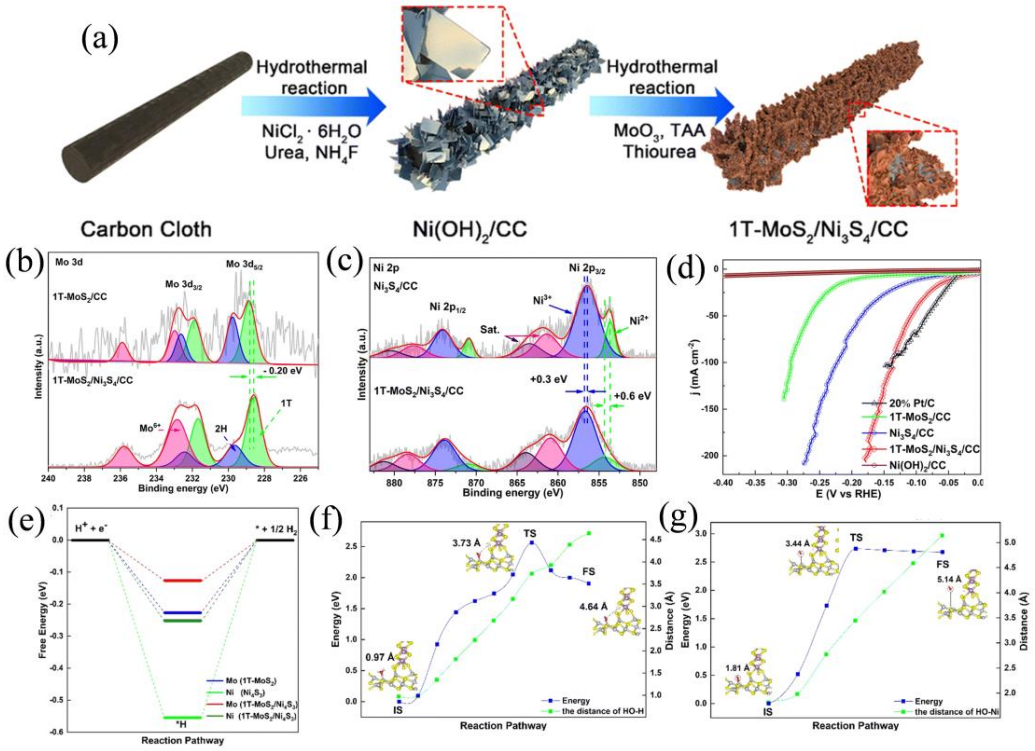

Figure 13. (**a**) Schematic illustrations of the synthesis protocols for 1T-MoS_2/Ni_3S_4/CC. XPS spectra of (**b**) Mo 3d (The green area represents the 1T phase, the blue area represents the 2H phase, and the red area represents the Mo^{6+}.) and (**c**) Ni 2p (The green area represents the Ni^{2+}, the blue area represents the Ni^{3+}, and the red and purple areas represent the satellite peaks.) of 1T-MoS_2/Ni_3S_4/CC. (**d**) Polarization curves in 1 M KOH and (**e**) free energy diagram of the HER of catalysts. (**f**) Activation energies for water dissociation and (**g**) hydroxyl desorption on 1T-MoS_2/Ni_3S_4, with energy along the reaction coordinate relative to each initial state (IS), transition state (TS), and final state (FS). Reproduced with permission from Ref. [75], Copyright 2023, Royal Society of Chemistry.

Wu et al. [73] grew a MoS_2/Co_9S_8 heterostructure on carbon cloth through a sulfur–sulfur combination and successfully obtained $MoS_2@Co_9S_8/CC$. Figure 14a–c shows that compared to MoS_2/CC and Co_9S_8/CC, the peak of Mo^{4+} has a negative shift (232.4 eV/232.1 eV to 229.2 eV/228.8 eV), and the peak of Co^{2+} has a positive shift (781.0 eV/797.1 eV to 781.4 eV/797.5 eV), which indicates that electrons are transferred from Co to Mo. The increased electrons around Mo are beneficial to improving the HER activity of the material [76]. Figure 14d shows that the overpotential of $MoS_2@Co_9S_8/CC$ at 10 mA cm^{-2} is only 73 mV in 1 M KOH solution, which is much lower than that of Co_9S_8/CC (199 mV), MoS_2/CC (157 mV), and CC (373 mV). It indicates that the $MoS_2/Co9S_8$ heterostructure greatly improves the HER activity of Co_9S_8 and MoS_2.

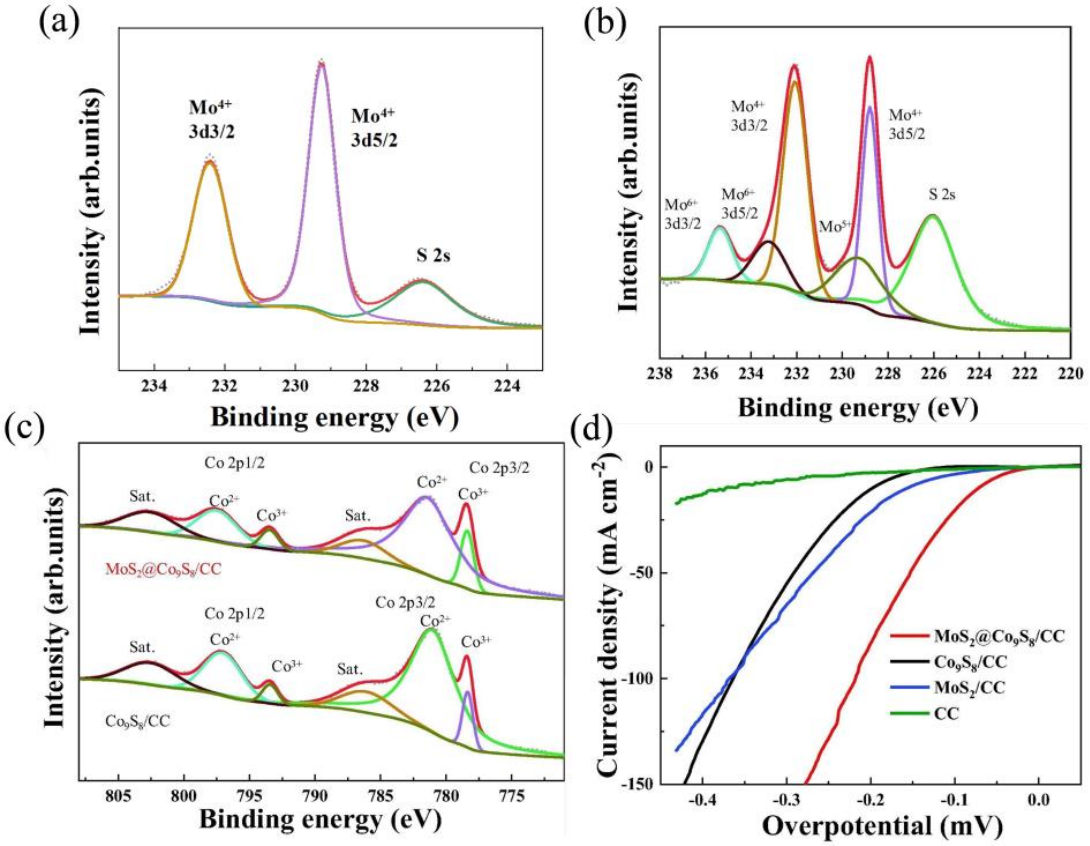

Figure 14. XPS spectra of Mo 3d of (**a**) MoS_2/CC and (**b**) $MoS_2@Co_9S_8/CC$. (**c**) XPS spectra of Co 2p of $MoS_2@Co_9S_8/CC$ and Co_9S_8/CC. (**d**) Polarization curves of catalysts in 1 M KOH. Reproduced with permission from Ref. [73], Copyright 2021, Elsevier.

Although great progress has been made in developing heterostructures containing MoS_2 for the electrolysis of water for hydrogen evolution, the catalytic mechanism is not clear. Synergistic effects are often used in the literature to explain the excellent performance of heterostructures for hydrogen evolution by electrolysis of water. More research is needed in the future to explain the interaction between heterogeneous interfaces to further clarify how the synergistic effects occur.

3.2. Conductive Substrate

Growing MoS_2 on a substrate with high electrical conductivity will significantly change the electronic structure and conductivity at the interface of the composite material, which can also optimize the intermediate adsorption energy on the catalyst surface and then obtain high-performance HER materials [77,78]. Commonly used conductive substrates include carbon materials and pure metals [79].

Carbon material is the preferred substrate because of its high conductivity and strong electron-donating ability. Hu et al. [80] first pretreated the conductive substrate carbon fiber paper (CFP) in nitric acid to make it smooth. Then, $Ni(OH)_2$ was grown on CFP to obtain $Ni(OH)_2$/CFP, and the $Ni(OH)_2$ on CFP was further converted into NiS_2 by vulcanization reaction at 150 °C. Finally, MoS_2 nanosheets were covered on the surface of NiS_2 nanosheets at 200 °C to obtain NiS_2@MoS_2/CFP (Figure 15a). Figure 15b,c shows that the overpotential of NiS_2@MoS_2/CFP at 10 mA cm^{-2} is 95 mV and the Tafel slope is 65 mV dec^{-1} in 0.5 M H_2SO_4 solution, which is significantly lower than that of NiS_2/CFP (198 mV@10 mA cm^{-2} and 82 mV dec^{-1}). As a conductive substrate, CFP significantly improves the conductivity of the composite material NiS_2@MoS_2/CFP, which is beneficial to improve the HER performance of NiS_2@MoS_2/CFP.

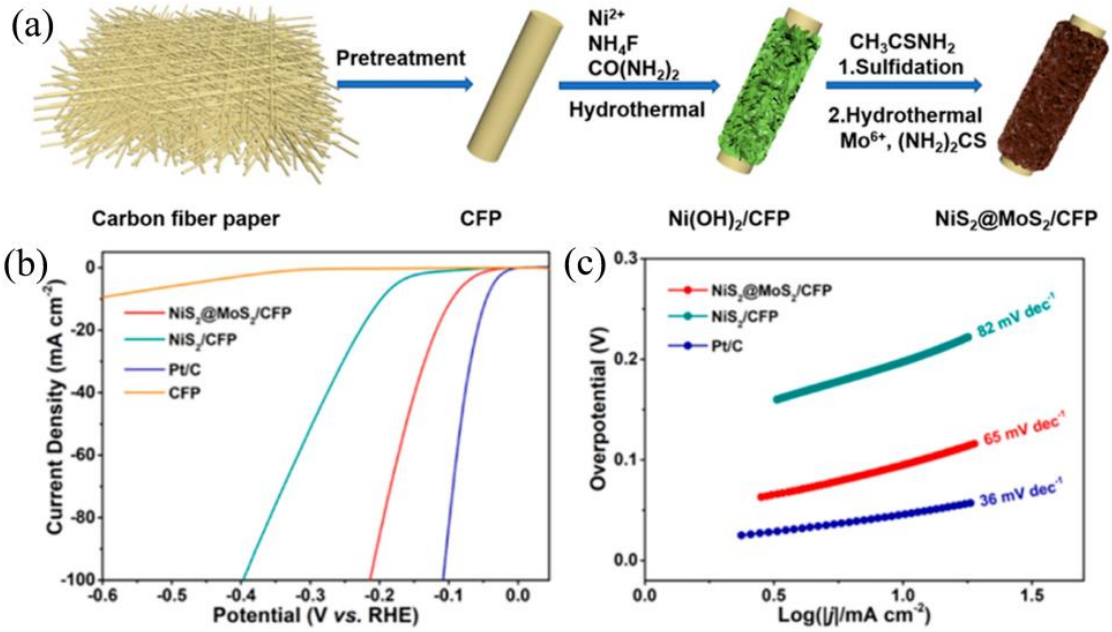

Figure 15. (**a**) Schematic illustrations of the synthesis protocols for NiS_2@MoS_2/CFP. (**b**) Polarization curves and (**c**) corresponding Tafel slopes of catalysts in 0.5 M H_2SO_4. Reproduced with permission from Ref. [80], Copyright 2022, American Chemical Society.

The metal substrate has good electrical conductivity. Thereby, the MoS_2 is also often grown on metal substrates to enhance its conductivity. Ma et al. [81] annealed Co-Fe PBA at 900 °C to obtain CoFe@NC and then introduced thiourea and sodium molybdate to anchor MoS_2 nanosheets on the surface of CoFe@NC to obtain MoS_2/CoFe@NC (Figure 16a). Figure 16b,c shows that the overpotential of MoS_2/CoFe@NC at 10 mA cm^{-2} is 172 mV and the Tafel slope is 122.4 mV dec^{-1} in 1.0 M KOH solution, which is significantly lower than that of CoFe@NC (266 mV@10 mA cm^{-2} and 111.6 mV dec^{-1}) and MoS_2 (330 mV@10 mA cm^{-2} and 214.0 mV dec^{-1}). The synergistic effect of the CoFe@NC substrate with abundant active sites and high conductivity and MoS_2 nanosheets accelerated the electron transfer rate, making MoS_2/CoFe@NC have excellent catalytic activity.

Current research focuses on using conductive substrates to improve the HER performance of MoS_2 while paying less attention to the stability of the interface between MoS_2 and the conductive substrate, and the loading of MoS_2. Good interface stability can improve the electron transfer rate and catalytic activity, but an unstable interface may lead to the exfoliation or agglomeration of MoS_2 nanoparticles and cause HER performance to decline. It is very important to load the appropriate amount of MoS_2 on the conductive substrate. Excessive loading may lead to mass transfer barriers between MoS_2 nanoparticles. If the loading amount is too small, the catalytic performance of MoS_2 may not be fully exerted. Future research should focus on solving these issues.

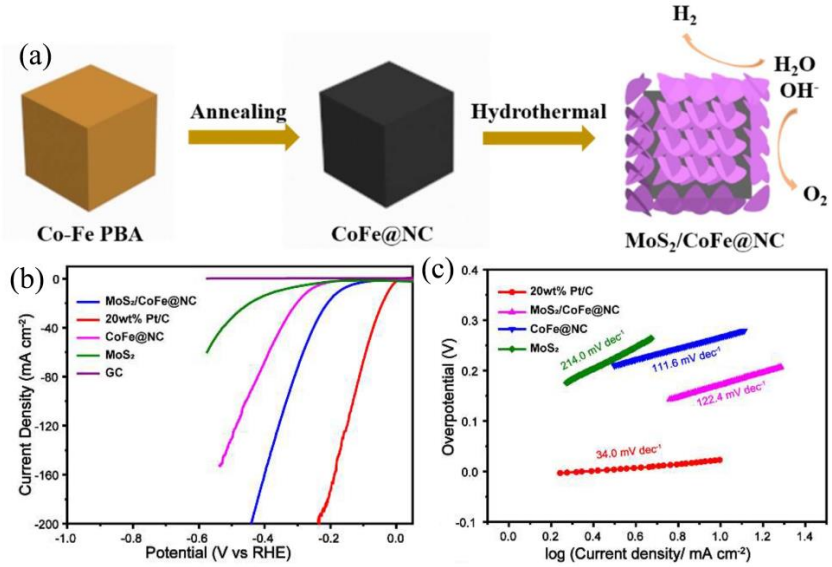

Figure 16. (**a**) Schematic illustrations of the synthesis protocols of MoS_2/CoFe@NC. (**b**) Polarization curves and (**c**) corresponding Tafel slopes of catalysts in 1.0 M KOH. Reproduced with permission from Ref. [81], Copyright 2023, Elsevier.

4. Conclusions and Outlook

This work summarizes the regulation strategies of MoS_2 from two aspects: internal modification and external modification. These regulation strategies include interlayer spacing, sulfur vacancy, phase transition, element doping, heterostructure, and conductive substrate. Figure 17 and Table 1 summarize the data for examples corresponding to the above regulation strategies. Although the HER performance of MoS_2 that has been modified using these strategies has been significantly improved, there are still some problems that need to be solved before large-scale industrial application.

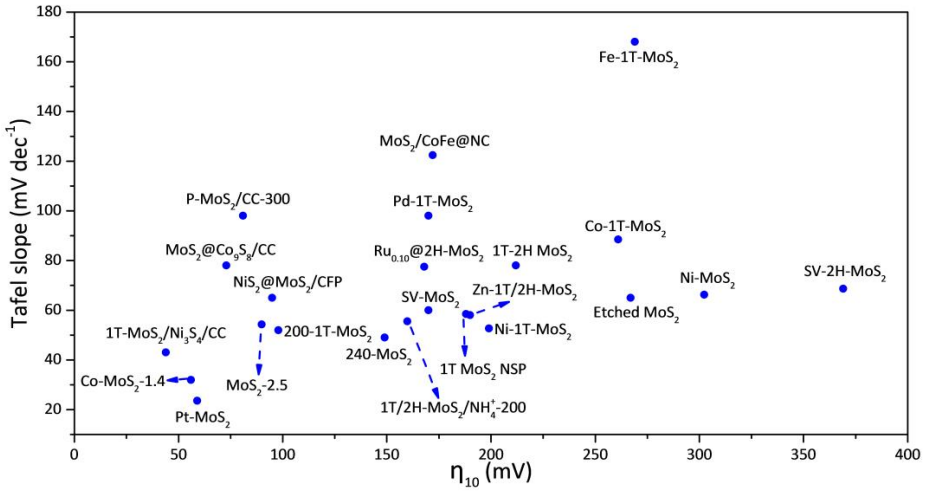

Figure 17. Comparison of performance of MoS_2 catalysts obtained using different modification strategies (200-1T-MoS_2 [36], 1T/2H-MoS_2/NH_4^+-200 [37], Co-MoS_2-1.4 [35], 240-MoS_2 [38], SV-2H-MoS_2 [42], MoS_2-2.5 [43], SV-MoS_2 [45], 1T MoS_2 NSP [55], 1T-2H MoS_2 [56], Ni-MoS_2 [60], Zn-1T/2H-MoS_2 [61], $Ru_{0.10}$@2H-MoS_2 [62], Fe-1T-MoS_2 [6], Co-1T-MoS_2 [6], Ni-1T-MoS_2 [6], Pt-MoS_2 [63], Pd-1T-MoS_2 [64], Etched MoS_2 [66], P-MoS_2/CC-300 [67], 1T-MoS_2/Ni_3S_4/CC [75], MoS_2@Co_9S_8/CC [73], NiS_2@MoS_2/CFP [80], MoS_2/CoFe@NC [81]).

First of all, the 1T phase has obvious advantages compared with the 2H phase in the field of electrolysis of water for hydrogen evolution. However, the metastable 1T phase

easily transforms into the thermodynamically stable 2H phase, resulting in a decrease in the HER performance of MoS_2. Industrial applications require catalysts with excellent long-term stability rather than being limited to dozens of hours in the laboratory. Research on how to maintain the 1T phase stability of MoS_2 is of great value for industrial applications. Secondly, single-atom catalysts have broad application prospects in the field of electrolysis of water for hydrogen evolution. At present, the loading of metal single atoms on the MoS_2 substrate is low. Increasing the loading of single atoms on the MoS_2 substrate can give full play to the catalytic efficiency of the atoms, and further improve the HER performance of the material. However, if the loading of metal atoms is too high, the metal atoms will easily form clusters. Future research should tend to increase the loading of metal single atoms on the MoS_2 substrate, so as to maximize the HER performance of the material while ensuring the single-atom state. Thirdly, loading MoS_2 on a conductive substrate can effectively improve the HER performance of MoS_2. The development of porous conductive substrates to support MoS_2 can not only improve the conductivity but also improve the mass transfer efficiency, which will fully enhance the HER performance of the material. Finally, in order to maximize the HER performance of MoS_2, two or more modification strategies discussed in this article may be combined.

Table 1. Summary of modification strategies for MoS_2 catalysts.

Strategy	Material	Electrolyte	η_{10} (mV)	Tafel Slope (mV dec^{-1})	Ref.
Interlayer spacing	200-1T-MoS_2	0.5 M H_2SO_4	98	52	[36]
	1T/2H-MoS_2/NH_4^+-200	0.5 M H_2SO_4	159.9	55.5	[37]
	Co-MoS_2-1.4	0.5 M H_2SO_4	56	32	[35]
	240-MoS_2	0.5 M H_2SO_4	149	49	[38]
Sulfur vacancy	SV-2H-MoS_2	0.5 M H_2SO_4	369	68.7	[42]
	MoS_2-2.5	0.5 M H_2SO_4	90	54.3	[43]
	SV-MoS_2	H_2SO_4 (pH = 0.2)	170	60	[45]
Phase transition	1T MoS_2 NSP	0.5 M H_2SO_4	188	58.47	[55]
	1T-2H MoS_2	0.5 M H_2SO_4	212	78	[56]
Metal doping	Ni-MoS_2	0.5 M H_2SO_4	302.4	66.27	[60]
	Zn-1T/2H-MoS_2	0.5 M H_2SO_4	190	58	[61]
	$Ru_{0.10}$@2H-MoS_2	0.5 M H_2SO_4	168	77.5	[62]
	Fe-1T-MoS_2	1.0 M KOH	269	168	[6]
	Co-1T-MoS_2	1.0 M KOH	261	88.5	
	Ni-1T-MoS_2	1.0 M KOH	199	52.7	
	Pt-MoS_2	0.5 M H_2SO_4	59	23.58	[63]
	Pd-1T-MoS_2	0.5 M H_2SO_4	170	98	[64]
Nonmetal doping	Etched MoS_2	0.5 M H_2SO_4	267	65	[66]
	P-MoS_2/CC-300	0.5 M H_2SO_4	81	98	[67]
Heterostructure	1T-MoS_2/Ni_3S_4/CC	1 M KOH	44	43	[75]
	MoS_2@Co_9S_8/CC	1 M KOH	73	78	[73]
Conductive substrate	NiS_2@MoS_2/CFP	0.5 M H_2SO_4	95	65	[80]
	MoS_2/CoFe@NC	1 M KOH	172	122.4	[81]

In general, there is still a lot of room for development in the field of MoS_2 towards electrocatalytic hydrogen evolution. With an in-depth understanding of material properties and continuous technological innovation, MoS_2 is expected to become an important catalyst in the field of clean energy, promoting the progress and sustainable development of water-splitting technology.

Author Contributions: L.L.: writing (preparation of the original draft) and methodology. N.L.: writing review and editing. C.D.: data curation and conceptualization. N.W.: Formal analysis. B.C.: supervision and validation. All authors have read and agreed to the published version of the manuscript.

Funding: National Key Research and Development Program of China (2023YFB4004703).

Data Availability Statement: Not applicable.

Conflicts of Interest: The authors declare no conflicts of interest.

References

1. Wu, H.; Feng, C.; Zhang, L.; Zhang, J.; Wilkinson, D.P. Non-noble Metal Electrocatalysts for the Hydrogen Evolution Reaction in Water Electrolysis. *Electrochem. Energy Rev.* **2021**, *4*, 473–507. [CrossRef]
2. Xiao, F.X.; Miao, J.; Tao, H.B.; Hung, S.F.; Wang, H.Y.; Yang, H.B.; Chen, J.; Chen, R.; Liu, B. One-dimensional hybrid nanostructures for heterogeneous photocatalysis and photoelectrocatalysis. *Small* **2015**, *11*, 2115–2131. [CrossRef] [PubMed]
3. Yu, Z.; Liu, H.; Zhu, M.; Li, Y.; Li, W. Interfacial Charge Transport in 1D TiO_2 Based Photoelectrodes for Photoelectrochemical Water Splitting. *Small* **2021**, *17*, 1903378. [CrossRef] [PubMed]
4. Zou, X.; Zhang, Y. Noble metal-free hydrogen evolution catalysts for water splitting. *Chem. Soc. Rev.* **2015**, *44*, 5148–5180. [CrossRef] [PubMed]
5. Ma, Y.; Leng, D.; Zhang, X.; Fu, J.; Pi, C.; Zheng, Y.; Gao, B.; Li, X.; Li, N.; Chu, P.K.; et al. Enhanced Activities in Alkaline Hydrogen and Oxygen Evolution Reactions on MoS_2 Electrocatalysts by In-Plane Sulfur Defects Coupled with Transition Metal Doping. *Small* **2022**, *18*, 2203173. [CrossRef] [PubMed]
6. Wang, G.; Zhang, G.; Ke, X.; Chen, X.; Chen, X.; Wang, Y.; Huang, G.; Dong, J.; Chu, S.; Sui, M. Direct Synthesis of Stable 1T-MoS_2 Doped with Ni Single Atoms for Water Splitting in Alkaline Media. *Small* **2022**, *18*, 2107238. [CrossRef] [PubMed]
7. He, P.; Yu, X.Y.; Lou, X.W. Carbon-Incorporated Nickel-Cobalt Mixed Metal Phosphide Nanoboxes with Enhanced Electrocatalytic Activity for Oxygen Evolution. *Angew. Chem. Int. Ed.* **2017**, *56*, 3897–3900. [CrossRef] [PubMed]
8. Liang, H.; Gandi, A.N.; Anjum, D.H.; Wang, X.; Schwingenschlogl, U.; Alshareef, H.N. Plasma-Assisted Synthesis of NiCoP for Efficient Overall Water Splitting. *Nano Lett.* **2016**, *16*, 7718–7725. [CrossRef]
9. Norskov, J.K.; Christensen, C.H. Chemistry. Toward efficient hydrogen production at surfaces. *Science* **2006**, *312*, 1322–1323. [CrossRef]
10. Zhang, Z.; Cong, L.; Yu, Z.; Qu, L.; Huang, W. Facile synthesis of Fe–Ni bimetallic N-doped carbon framework for efficient electrochemical hydrogen evolution reaction. *Mater. Today Energy* **2020**, *16*, 100387. [CrossRef]
11. Zhang, J.; Wang, T.; Liu, P.; Liu, S.; Dong, R.; Zhuang, X.; Chen, M.; Feng, X. Engineering water dissociation sites in MoS_2 nanosheets for accelerated electrocatalytic hydrogen production. *Energy Environ. Sci.* **2016**, *9*, 2789–2793. [CrossRef]
12. Dai, X.; Du, K.; Li, Z.; Liu, M.; Ma, Y.; Sun, H.; Zhang, X.; Yang, Y. Co-Doped MoS_2 Nanosheets with the Dominant CoMoS Phase Coated on Carbon as an Excellent Electrocatalyst for Hydrogen Evolution. *ACS Appl. Mater. Interfaces* **2015**, *7*, 27242–27253. [CrossRef] [PubMed]
13. Wu, K.; Li, X.; Wang, W.; Huang, Y.; Jiang, Q.; Li, W.; Chen, Y.; Yang, Y.; Li, C. Creating Edge Sites within the Basal Plane of a MoS_2 Catalyst for Substantially Enhanced Hydrodeoxygenation Activity. *ACS Catal.* **2021**, *12*, 8–17. [CrossRef]
14. Xie, Y.; Chen, L.; Jin, Q.; Yun, J.; Liang, X. MoS_2–Co_3S_4 hollow polyhedrons derived from ZIF-67 towards hydrogen evolution reaction and hydrodesulfurization. *Int. J. Hydrog. Energy* **2019**, *44*, 24246–24255. [CrossRef]
15. Gao, G.; Jiao, Y.; Ma, F.; Jiao, Y.; Waclawik, E.; Du, A. Charge Mediated Semiconducting-to-Metallic Phase Transition in Molybdenum Disulfide Monolayer and Hydrogen Evolution Reaction in New 1T′ Phase. *J. Phys. Chem. C* **2015**, *119*, 13124–13128. [CrossRef]
16. Liu, Q.; Li, X.; He, Q.; Khalil, A.; Liu, D.; Xiang, T.; Wu, X.; Song, L. Gram-Scale Aqueous Synthesis of Stable Few-Layered 1T-MoS_2: Applications for Visible-Light-Driven Photocatalytic Hydrogen Evolution. *Small* **2015**, *11*, 5556–5564. [CrossRef] [PubMed]
17. Lukowski, M.A.; Daniel, A.S.; Meng, F.; Forticaux, A.; Li, L.; Jin, S. Enhanced hydrogen evolution catalysis from chemically exfoliated metallic MoS_2 nanosheets. *J. Am. Chem. Soc.* **2013**, *135*, 10274–10277. [CrossRef] [PubMed]
18. Zhu, C.R.; Gao, D.; Ding, J.; Chao, D.; Wang, J. TMD-based highly efficient electrocatalysts developed by combined computational and experimental approaches. *Chem. Soc. Rev.* **2018**, *47*, 4332–4356. [CrossRef]
19. Jin, Q.; Liu, N.; Chen, B.; Mei, D. Mechanisms of Semiconducting 2H to Metallic 1T Phase Transition in Two-dimensional MoS_2 Nanosheets. *J. Phys. Chem. C* **2018**, *122*, 28215–28224. [CrossRef]
20. Benson, E.E.; Zhang, H.; Schuman, S.A.; Nanayakkara, S.U.; Bronstein, N.D.; Ferrere, S.; Blackburn, J.L.; Miller, E.M. Balancing the Hydrogen Evolution Reaction, Surface Energetics, and Stability of Metallic MoS_2 Nanosheets via Covalent Functionalization. *J. Am. Chem. Soc.* **2018**, *140*, 441–450. [CrossRef]
21. Venkateshwaran, S.; Senthil Kumar, S.M. Provoking Metallic 1T Phase Conversion of 2H-MoS_2 via an Effectual Solvothermal Route for Electrocatalytic Water Reduction in Acid. *ACS Sustain. Chem. Eng.* **2022**, *10*, 5258–5267. [CrossRef]
22. Cai, L.; Cheng, W.; Yao, T.; Huang, Y.; Tang, F.; Liu, Q.; Liu, W.; Sun, Z.; Hu, F.; Jiang, Y.; et al. High-Content Metallic 1T Phase in MoS_2-Based Electrocatalyst for Efficient Hydrogen Evolution. *J. Phys. Chem. C* **2017**, *121*, 15071–15077. [CrossRef]
23. Wang, D.; Zhang, X.; Bao, S.; Zhang, Z.; Fei, H.; Wu, Z. Phase engineering of a multiphasic 1T/2H MoS_2 catalyst for highly efficient hydrogen evolution. *J. Mater. Chem. A* **2017**, *5*, 2681–2688. [CrossRef]
24. Li, L.; Qin, Z.; Ries, L.; Hong, S.; Michel, T.; Yang, J.; Salameh, C.; Bechelany, M.; Miele, P.; Kaplan, D.; et al. Role of Sulfur Vacancies and Undercoordinated Mo Regions in MoS_2 Nanosheets toward the Evolution of Hydrogen. *ACS Nano* **2019**, *13*, 6824–6834. [CrossRef] [PubMed]
25. Geng, S.; Yang, W.; Liu, Y.; Yu, Y. Engineering sulfur vacancies in basal plane of MoS_2 for enhanced hydrogen evolution reaction. *J. Catal.* **2020**, *391*, 91–97. [CrossRef]
26. Tsai, C.; Li, H.; Park, S.; Park, J.; Han, H.S.; Nørskov, J.K.; Zheng, X.; Abild-Pedersen, F. Electrochemical generation of sulfur vacancies in the basal plane of MoS_2 for hydrogen evolution. *Nat. Commun.* **2017**, *8*, 15113. [CrossRef] [PubMed]

27. Zhang, J.; Xu, X.; Yang, L.; Cheng, D.; Cao, D. Single-Atom Ru Doping Induced Phase Transition of MoS_2 and S Vacancy for Hydrogen Evolution Reaction. *Small Methods* **2019**, *3*, 1900653. [CrossRef]
28. Deng, J.; Li, H.; Xiao, J.; Tu, Y.; Deng, D.; Yang, H.; Tian, H.; Li, J.; Ren, P.; Bao, X. Triggering the electrocatalytic hydrogen evolution activity of the inert two-dimensional MoS_2 surface via single-atom metal doping. *Energy Environ. Sci.* **2015**, *8*, 1594–1601. [CrossRef]
29. Li, R.; Yang, L.; Xiong, T.; Wu, Y.; Cao, L.; Yuan, D.; Zhou, W. Nitrogen doped MoS_2 nanosheets synthesized via a low-temperature process as electrocatalysts with enhanced activity for hydrogen evolution reaction. *J. Power Sources* **2017**, *356*, 133–139. [CrossRef]
30. Liu, Q.; Xue, Z.; Jia, B.; Liu, Q.; Liu, K.; Lin, Y.; Liu, M.; Li, Y.; Li, G. Hierarchical Nanorods of MoS_2/MoP Heterojunction for Efficient Electrocatalytic Hydrogen Evolution Reaction. *Small* **2020**, *16*, 2002482. [CrossRef]
31. Xiao, X.; Wang, Y.; Xu, X.; Yang, T.; Zhang, D. Preparation of the flower-like MoS_2/SnS_2 heterojunction as an efficient electrocatalyst for hydrogen evolution reaction. *Mol. Catal.* **2020**, *487*, 110890. [CrossRef]
32. Wu, A.; Tian, C.; Yan, H.; Jiao, Y.; Yan, Q.; Yang, G.; Fu, H. Hierarchical MoS_2@MoP core-shell heterojunction electrocatalysts for efficient hydrogen evolution reaction over a broad pH range. *Nanoscale* **2016**, *8*, 11052–11059. [CrossRef] [PubMed]
33. Wang, Q.; Zhao, Z.L.; Dong, S.; He, D.; Lawrence, M.J.; Han, S.; Cai, C.; Xiang, S.; Rodriguez, P.; Xiang, B.; et al. Design of active nickel single-atom decorated MoS_2 as a pH-universal catalyst for hydrogen evolution reaction. *Nano Energy* **2018**, *53*, 458–467. [CrossRef]
34. Liu, P.; Zhu, J.; Zhang, J.; Xi, P.; Tao, K.; Gao, D.; Xue, D. P Dopants Triggered New Basal Plane Active Sites and Enlarged Interlayer Spacing in MoS_2 Nanosheets toward Electrocatalytic Hydrogen Evolution. *ACS Energy Lett.* **2017**, *2*, 745–752. [CrossRef]
35. Jin, Q.; Liu, N.; Dai, C.; Xu, R.; Wu, B.; Yu, G.; Chen, B.; Du, Y. H_2-Directing Strategy on In Situ Synthesis of Co-MoS_2 with Highly Expanded Interlayer for Elegant HER Activity and its Mechanism. *Adv. Energy Mater.* **2020**, *10*, 2000291. [CrossRef]
36. Zhang, H.; Xu, H.; Wang, L.; Ouyang, C.; Liang, H.; Zhong, S. A Metal-Organic Frameworks Derived 1T-MoS_2 with Expanded Layer Spacing for Enhanced Electrocatalytic Hydrogen Evolution. *Small* **2023**, *19*, 2205736. [CrossRef] [PubMed]
37. Hu, W.; Liu, H.; Dong, W.; Akif Munir, H.; Fan, X.; Tian, X.; Pang, L. Ammonium ions intercalated 1T/2H-MoS_2 with increased interlayer spacing for high-efficient electrocatalytic hydrogen evolution reaction. *J. Electroanal. Chem.* **2023**, *949*, 117882. [CrossRef]
38. Gao, M.R.; Chan, M.K.; Sun, Y. Edge-terminated molybdenum disulfide with a 9.4-A interlayer spacing for electrochemical hydrogen production. *Nat. Commun.* **2015**, *6*, 7493. [CrossRef]
39. Bui, H.T.; Linh, D.C.; Nguyen, L.D.; Chang, H.; Patil, S.A.; Shrestha, N.K.; Bui, K.X.; Bui, T.S.; Nguyen, T.N.A.; Tung, N.T.; et al. In-situ formation and integration of graphene into MoS_2 interlayer spacing: Expansion of interlayer spacing for superior hydrogen evolution reaction in acidic and alkaline electrolyte. *J. Mater. Sci.* **2022**, *57*, 18993–19005. [CrossRef]
40. Lu, A.Y.; Yang, X.; Tseng, C.C.; Min, S.; Lin, S.H.; Hsu, C.L.; Li, H.; Idriss, H.; Kuo, J.L.; Huang, K.W.; et al. High-Sulfur-Vacancy Amorphous Molybdenum Sulfide as a High Current Electrocatalyst in Hydrogen Evolution. *Small* **2016**, *12*, 5530–5537. [CrossRef]
41. Cheng, C.-C.; Lu, A.-Y.; Tseng, C.-C.; Yang, X.; Hedhili, M.N.; Chen, M.-C.; Wei, K.-H.; Li, L.-J. Activating basal-plane catalytic activity of two-dimensional MoS_2 monolayer with remote hydrogen plasma. *Nano Energy* **2016**, *30*, 846–852. [CrossRef]
42. Gu, C.; Sun, T.; Wang, Z.; Jiang, S.; Wang, Z. High Resolution Electrochemical Imaging for Sulfur Vacancies on 2D Molybdenum Disulfide. *Small Methods* **2023**, *7*, 2201529. [CrossRef] [PubMed]
43. Man, P.; Jiang, S.; Leung, K.H.; Lai, K.H.; Guang, Z.; Chen, H.; Huang, L.; Chen, T.; Gao, S.; Peng, Y.K.; et al. Salt-Induced High-Density Vacancy-Rich 2D MoS_2 for Efficient Hydrogen Evolution. *Adv. Mater.* **2023**, *2023*, 2304808. [CrossRef] [PubMed]
44. Ye, G.; Gong, Y.; Lin, J.; Li, B.; He, Y.; Pantelides, S.T.; Zhou, W.; Vajtai, R.; Ajayan, P.M. Defects Engineered Monolayer MoS_2 for Improved Hydrogen Evolution Reaction. *Nano Lett.* **2016**, *16*, 1097–1103. [CrossRef] [PubMed]
45. Li, H.; Tsai, C.; Koh, A.L.; Cai, L.; Contryman, A.W.; Fragapane, A.H.; Zhao, J.; Han, H.S.; Manoharan, H.C.; Abild-Pedersen, F.; et al. Activating and optimizing MoS_2 basal planes for hydrogen evolution through the formation of strained sulphur vacancies. *Nat. Mater.* **2016**, *15*, 48–53. [CrossRef] [PubMed]
46. Bollinger, M.V.; Jacobsen, K.W.; Nørskov, J.K. Atomic and electronic structure of MoS_2 nanoparticles. *Phys. Rev. B* **2003**, *67*, 085410. [CrossRef]
47. Vojvodic, A.; Hinnemann, B.; Nørskov, J.K. Magnetic edge states in MoS_2 characterized using density-functional theory. *Phys. Rev. B* **2009**, *80*, 125416. [CrossRef]
48. Ali Shah, S.; Sayyar, R.; Xu, L.; Sun, H.; Khan, I.; Guo, J.; Shen, X.; Hussain, S.; Yuan, A.; Ullah, H. In-situ synthesis of NiS_2 nanoparticles/MoS_2 nanosheets hierarchical sphere anchored on reduced graphene oxide for enhanced electrocatalytic hydrogen evolution reaction. *J. Colloid Interface Sci.* **2022**, *624*, 150–159. [CrossRef]
49. Ali Shah, S.; Xu, L.; Sayyar, R.; Khan, I.; Yuan, A.; Shen, X.; Li, X.; Ullah, H. FeNi@N-Doped Graphene Core–Shell Nanoparticles on Carbon Matrix Coupled with MoS_2 Nanosheets as a Competent Electrocatalyst for Efficient Hydrogen Evolution Reaction. *Adv. Mater. Interfaces* **2022**, *9*, 2201040. [CrossRef]
50. Kibsgaard, J.; Chen, Z.; Reinecke, B.N.; Jaramillo, T.F. Engineering the surface structure of MoS_2 to preferentially expose active edge sites for electrocatalysis. *Nat. Mater.* **2012**, *11*, 963–969. [CrossRef]
51. Hinnemann, B.; Moses, P.G.; Bonde, J.; Jorgensen, K.P.; Nielsen, J.H.; Horch, S.; Chorkendorff, I.; Norskov, J.K. Biomimetic hydrogen evolution: MoS_2 nanoparticles as catalyst for hydrogen evolution. *J. Am. Chem. Soc.* **2005**, *127*, 5308–5309. [CrossRef] [PubMed]
52. Jaramillo, T.F.; Jorgensen, K.P.; Bonde, J.; Nielsen, J.H.; Horch, S.; Chorkendorff, I. Identification of active edge sites for electrochemical H_2 evolution from MoS_2 nanocatalysts. *Science* **2007**, *317*, 100–102. [CrossRef] [PubMed]

53. Voiry, D.; Salehi, M.; Silva, R.; Fujita, T.; Chen, M.; Asefa, T.; Shenoy, V.B.; Eda, G.; Chhowalla, M. Conducting MoS_2 nanosheets as catalysts for hydrogen evolution reaction. *Nano Lett.* **2013**, *13*, 6222–6227. [CrossRef]
54. Tang, Q.; Jiang, D.-E. Mechanism of Hydrogen Evolution Reaction on 1T-MoS_2 from First Principles. *ACS Catal.* **2016**, *6*, 4953–4961. [CrossRef]
55. Wang, S.; Li, Y.; Hu, Y.; Zhou, X.; Zhang, M.; Jia, X.; Yang, Y.; Lin, B.-L.; Chen, G. One-Step Synthesis of 1T MoS_2 Hierarchical Nanospheres for Electrocatalytic Hydrogen Evolution. *ACS Appl. Energy Mater.* **2022**, *5*, 11705–11712. [CrossRef]
56. Hong, Z.; Hong, W.; Wang, B.; Cai, Q.; He, X.; Liu, W. Stable 1T–2H MoS_2 heterostructures for efficient electrocatalytic hydrogen evolution. *Chem. Eng. J.* **2023**, *460*, 141858. [CrossRef]
57. Zhang, H.; Yu, L.; Chen, T.; Zhou, W.; Lou, X.W. Surface Modulation of Hierarchical MoS_2 Nanosheets by Ni Single Atoms for Enhanced Electrocatalytic Hydrogen Evolution. *Adv. Funct. Mater.* **2018**, *28*, 1807086. [CrossRef]
58. Luo, Z.; Ouyang, Y.; Zhang, H.; Xiao, M.; Ge, J.; Jiang, Z.; Wang, J.; Tang, D.; Cao, X.; Liu, C.; et al. Chemically activating MoS_2 via spontaneous atomic palladium interfacial doping towards efficient hydrogen evolution. *Nat. Commun.* **2018**, *9*, 2120. [CrossRef]
59. Shi, Y.; Zhou, Y.; Yang, D.R.; Xu, W.X.; Wang, C.; Wang, F.B.; Xu, J.J.; Xia, X.H.; Chen, H.Y. Energy Level Engineering of MoS_2 by Transition-Metal Doping for Accelerating Hydrogen Evolution Reaction. *J. Am. Chem. Soc.* **2017**, *139*, 15479–15485. [CrossRef]
60. Sundara Venkatesh, P.; Kannan, N.; Ganesh Babu, M.; Paulraj, G.; Jeganathan, K. Transition metal doped MoS_2 nanosheets for electrocatalytic hydrogen evolution reaction. *Int. J. Hydrog. Energy* **2022**, *47*, 37256–37263. [CrossRef]
61. Xu, J.; Zhao, Z.; Wei, W.; Chang, G.; Xie, Z.; Guo, W.; Liu, D.; Qu, D.; Tang, H.; Li, J. Tuning the Intrinsic Activity and Electrochemical Surface Area of MoS_2 via Tiny Zn Doping: Toward an Efficient Hydrogen Evolution Reaction (HER) Catalyst. *Chem. Eur. J.* **2021**, *27*, 15992–15999. [CrossRef] [PubMed]
62. Wang, J.; Fang, W.; Hu, Y.; Zhang, Y.; Dang, J.; Wu, Y.; Chen, B.; Zhao, H.; Li, Z. Single atom Ru doping 2H-MoS_2 as highly efficient hydrogen evolution reaction electrocatalyst in a wide pH range. *Appl. Catal. B Environ.* **2021**, *298*, 120490. [CrossRef]
63. Pei, L.; Qiao, H.; Chen, B.; Zhu, X.; Davis, R.A.; Zhu, K.; Xia, L.; Dong, P.; Ye, M.; Shen, J. Pt Edge-Doped MoS_2: Activating the Active Sites for Maximized Hydrogen Evolution Reaction Performance. *Small* **2021**, *17*, 2104245. [CrossRef] [PubMed]
64. Song, X.; Li, B.; Peng, W.; Wang, C.; Li, K.; Zhu, Y.; Mei, Y. A palladium doped 1T-phase molybdenum disulfide–black phosphorene two-dimensional van der Waals heterostructure for visible-light enhanced electrocatalytic hydrogen evolution. *Nanoscale* **2021**, *13*, 5892–5900. [CrossRef] [PubMed]
65. Wang, Y.; Liu, S.; Hao, X.; Zhou, J.; Song, D.; Wang, D.; Hou, L.; Gao, F. Fluorine- and Nitrogen-Codoped MoS_2 with a Catalytically Active Basal Plane. *ACS Appl. Mater. Interfaces* **2017**, *9*, 27715–27719. [CrossRef] [PubMed]
66. Zhang, R.; Zhang, M.; Yang, H.; Li, G.; Xing, S.; Li, M.; Xu, Y.; Zhang, Q.; Hu, S.; Liao, H.; et al. Creating Fluorine-Doped MoS_2 Edge Electrodes with Enhanced Hydrogen Evolution Activity. *Small Methods* **2021**, *5*, 2100612. [CrossRef] [PubMed]
67. Tian, J.; Yang, C.; Hao, R.; Li, F.; Liu, Z.; Chen, W.; Lv, Y.; Lin, C. Fabrication of phosphorus-mediated MoS_2 nanosheets on carbon cloth for enhanced hydrogen evolution reaction. *Int. J. Hydrog. Energy* **2022**, *47*, 17871–17878. [CrossRef]
68. Yin, Y.; Han, J.; Zhang, Y.; Zhang, X.; Xu, P.; Yuan, Q.; Samad, L.; Wang, X.; Wang, Y.; Zhang, Z.; et al. Contributions of Phase, Sulfur Vacancies, and Edges to the Hydrogen Evolution Reaction Catalytic Activity of Porous Molybdenum Disulfide Nanosheets. *J. Am. Chem. Soc.* **2016**, *138*, 7965–7972. [CrossRef]
69. Wang, J.; Yan, M.; Zhao, K.; Liao, X.; Wang, P.; Pan, X.; Yang, W.; Mai, L. Field Effect Enhanced Hydrogen Evolution Reaction of MoS_2 Nanosheets. *Adv. Mater.* **2017**, *29*, 1604464. [CrossRef]
70. Guo, Y.; Gan, L.; Shang, C.; Wang, E.; Wang, J. A Cake-Style CoS_2@MoS_2/RGO Hybrid Catalyst for Efficient Hydrogen Evolution. *Adv. Funct. Mater.* **2016**, *27*, 1602699. [CrossRef]
71. Chen, W.; Gu, J.; Du, Y.; Song, F.; Bu, F.; Li, J.; Yuan, Y.; Luo, R.; Liu, Q.; Zhang, D. Achieving Rich and Active Alkaline Hydrogen Evolution Heterostructures via Interface Engineering on 2D 1T-MoS_2 Quantum Sheets. *Adv. Funct. Mater.* **2020**, *30*, 2000551. [CrossRef]
72. Jia, Y.; Zhang, L.; Gao, G.; Chen, H.; Wang, B.; Zhou, J.; Soo, M.T.; Hong, M.; Yan, X.; Qian, G.; et al. A Heterostructure Coupling of Exfoliated Ni-Fe Hydroxide Nanosheet and Defective Graphene as a Bifunctional Electrocatalyst for Overall Water Splitting. *Adv. Mater.* **2017**, *29*, 1700017. [CrossRef] [PubMed]
73. Wu, J.; Wang, X.; Jiang, J.; Lin, W.; Zhu, S.; Sha, J.; Ma, L.; Zhao, N. In-situ synthesis of MoS_2/Co_9S_8 heterostructure for efficient HER electrocatalyst. *Mater. Lett.* **2021**, *292*, 129621. [CrossRef]
74. Hao, J.; Hu, H.; Dong, Y.; Hu, J.; Sang, X.; Duan, F.; Lu, S.; Zhu, H.; Du, M. Interface engineering in core–shell Co_9S_8@MoS_2 nanocrystals induces enhanced hydrogen evolution in acidic and alkaline media. *New J. Chem.* **2021**, *45*, 11167–11173. [CrossRef]
75. Xiang, L.; Liu, X.; Xu, S.; Wang, K.; Yuan, S.; Li, N. Constructing a 1T-MoS_2/Ni_3S_4 heterostructure to balance water dissociation and hydroxyl desorption for efficient hydrogen evolution. *Catal. Sci. Technol.* **2023**, *13*, 3901–3909. [CrossRef]
76. Kim, M.; Anjum, M.A.R.; Choi, M.; Jeong, H.Y.; Choi, S.H.; Park, N.; Lee, J.S. Covalent 0D–2D Heterostructuring of Co_9S_8–MoS_2 for Enhanced Hydrogen Evolution in All pH Electrolytes. *Adv. Funct. Mater.* **2020**, *30*, 2002536. [CrossRef]
77. Tang, J.; Huang, J.; Ding, D.; Zhang, S.; Deng, X. Research progress of 1T-MoS_2 in electrocatalytic hydrogen evolution. *Int. J. Hydrog. Energy* **2022**, *47*, 39771–39795. [CrossRef]
78. Wang, H.; Lin, Y.; Liu, S.; Li, J.; Bu, L.; Chen, J.; Xiao, X.; Choi, J.-H.; Gao, L.; Lee, J.-M. Confined growth of pyridinic N–Mo_2C sites on MXenes for hydrogen evolution. *J. Mater. Chem. A* **2020**, *8*, 7109–7116. [CrossRef]
79. Li, G.; Chen, Z.; Li, Y.; Zhang, D.; Yang, W.; Liu, Y.; Cao, L. Engineering Substrate Interaction To Improve Hydrogen Evolution Catalysis of Monolayer MoS_2 Films beyond Pt. *ACS Nano* **2020**, *14*, 1707–1714. [CrossRef]

80. Hu, H.; Xu, J.; Zheng, Y.; Zhu, Y.; Rong, J.; Zhang, T.; Yang, D.; Qiu, F. NiS_2-Coated Carbon Fiber Paper Decorated with MoS_2 Nanosheets for Hydrogen Evolution. *ACS Appl. Nano Mater.* **2022**, *5*, 10933–10940. [CrossRef]
81. Ma, W.; Li, W.; Zhang, H.; Wang, Y. N-doped carbon wrapped CoFe alloy nanoparticles with MoS_2 nanosheets as electrocatalyst for hydrogen and oxygen evolution reactions. *Int. J. Hydrog. Energy* **2023**, *48*, 22032–22043. [CrossRef]